

1  
2 **Deep ocean mass fluxes in the coastal upwelling off Mauritania from 1988 to 2012:**  
3 **variability on seasonal to decadal timescales**  
4

5  
6 *Fischer, G.,<sup>1,2\*</sup>, Romero, O.<sup>2</sup>, Merkel, U.<sup>1,2</sup>, Donner, B.<sup>2</sup>, Iversen, M.<sup>2,3</sup>, Nowald, N.<sup>2</sup>, Ratmeyer, V.<sup>2</sup>,*  
7 *Ruhland, G.<sup>2</sup>, Klann, M.<sup>2</sup> and G. Wefer<sup>2</sup>*  
8

9  
10 <sup>1</sup> Geosciences Department, University of Bremen, Klagenfurter Str,  
11 28359 Bremen, Germany  
12

13 <sup>2</sup> Marum Center for Marine and Environmental Sciences, Leobener Str,  
14 28359 Bremen, Germany  
15

16 <sup>3</sup> Alfred Wegener Institute for Polar and Marine Research, Am Handelshafen,  
17 27570 Bremerhaven, Germany  
18

19 \* *corresponding author*  
20  
21

**22 Abstract**

23 A more than two-decadal sediment trap record from the Eastern Boundary Upwelling Ecosystem (EBUE) off  
24 Cape Blanc, Mauritania, is analysed with respect to deep ocean mass fluxes, flux components and their  
25 variability on seasonal to decadal timescales. The total mass flux revealed interannual fluctuations which  
26 were superimposed by fluctuations on decadal timescales. High winter fluxes of biogenic silica (BSi), used  
27 as a measure of marine production (mostly by diatoms) largely correspond to a positive North Atlantic  
28 Oscillation (NAO) index (Dec.-March). However, this relationship is weak. The highest positive BSi  
29 anomaly was in winter 2004-2005 when the NAO was in a neutral state. More episodic BSi sedimentation  
30 events occurred in several summer seasons between 2001 and 2005, when the previous winter NAO was  
31 neutral or even negative. We suggest that distinct dust outbreaks and deposition in the surface ocean in  
32 winter and occasionally in summer/fall enhanced particle sedimentation and carbon export on short  
33 timescales via the ballasting effect. Episodic perturbations of the marine carbon cycle by dust outbreaks (e.g.  
34 in 2005) might have weakened the relationships between fluxes and large scale climatic oscillations. As  
35 phytoplankton biomass is high throughout the year, any dry (in winter) or wet (in summer) deposition of  
36 fine-grained dust particles is assumed to enhance the efficiency of the biological pump by incorporating dust  
37 into dense and fast settling organic-rich aggregates. A good correspondence between BSi and dust fluxes was  
38 observed for the dusty year 2005, following a period of rather dry conditions in the Sahara/Sahel region.  
39 Large changes of all bulk fluxes occurred during the strongest El Niño-Southern Oscillation (ENSO) in  
40 1997-1999 where low fluxes were obtained for almost one year during the warm El Niño and high fluxes in  
41 the following cold La Niña phase. For decadal timescales, Bakun (1990) suggested an intensification of  
42 coastal upwelling due to increased winds ('Bakun upwelling intensification hypothesis'; Cropper et al.,  
43 2014) and global climate change. We did not observe an increase of any flux component off Cape Blanc  
44 during the past two and a half decades which might support this. Furthermore, fluxes of mineral dust did not  
45 show any positive or negative trends over time which might suggest enhanced desertification or 'Saharan  
46 greening' during the last few decades.

47

48

## 49 **1. Introduction**

50 Eastern Boundary Upwelling Ecosystems (EBUEs; Freon et al., 2009) cover only about 1% of the total  
51 ocean area but contribute with about 15% to total marine primary production (Carr, 2002; Behrenfeld and  
52 Falkowski, 1997). Roughly, 20% of the marine global fish catch is provided by the four major EBUEs (Pauly  
53 and Christensen, 1995), the Benguela, the Canary, the Californian and the Humboldt Current Systems.  
54 Continental margins may be responsible for more than 40% of the carbon sequestration in the ocean (Muller-  
55 Karger et al., 2005) and are thus, highly relevant for the global carbon cycle. In the literature, multiple  
56 factors with potential influence on upwelling systems have been mentioned. To discuss all of them, would be  
57 beyond the scope of this paper and we therefore focus on three major factors.

58 In the 1990s, a discussion began whether global warming may lead to intensified coastal upwelling in the  
59 EBUEs (e.g. Bakun, 1990: ‘Bakun upwelling intensification hypothesis’; Cropper et al., 2014). Since then,  
60 various studies showed contradicting results, depending on the timescales regarded, the area studied and the  
61 methods applied. The longer-term time series analysis of wind stress and sea surface temperature (SST) by  
62 Narayan et al. (2014) from coastal upwelling areas seems to support the ‘Bakun upwelling intensification  
63 hypothesis’, but correlation analysis showed ambiguous results concerning the relationships of upwelling to  
64 the North Atlantic Oscillation (NAO). With some modification, the ‘Bakun hypothesis’ is supported for the  
65 Canary Current (CC) coastal upwelling system by Cropper et al. (2014). Using an upwelling index derived  
66 from SSTs and remote sensing wind stress, Marcello et al. (2011) obtained increased offshore spreading of  
67 upwelled waters off Cape Blanc from 1987 to 2006. Other authors, however, found a warming trend of the  
68 Canary Current System (e.g. Aristegui et al., 2009). Bode et al. (2009) observed a continuous decrease in  
69 upwelling intensity in the northern CC around the Canary Islands during the past 40 years, associated with  
70 the warming of surface waters, a decrease in zooplankton abundance, and, locally, in phytoplankton  
71 abundance. Studying a sediment core off Cape Ghir, Morocco, a cooling of the northern Canary Current in  
72 the 20<sup>th</sup> century was inferred (McGregor et al. 2007).

73 An influence of tropical Pacific interannual variability on EBUEs has also been proposed earlier. A link  
74 between the cold La Niña period (1997-1999 ENSO cycle) and the Mauritanian upwelling via a  
75 strengthening of the north-easterly (NE) trade winds in fall and winter was described by Pradhan et al.  
76 (2006). Helmke et al. (2005) correlated these anomalous events with deep-ocean carbon fluxes at the  
77 mesotrophic Cape Blanc study site. Using ocean colour data, Fischer et al. (2009) showed a large extension  
78 of the Cape Blanc filament from fall 1998 to spring 1999 when comparing it to the rest of the record (1997-  
79 2008). Using remote sensing data, Nykjaer and Van Camp (1994) found a weak northwest upwelling south  
80 of 20°N during and after the strong 1982-1983 El Niño event.

81 The NW African margin and the low-latitude North Atlantic are heavily influenced by Saharan dust  
82 transport, deposition (e.g. Kaufman et al., 2005) and sedimentation (Brust et al., 2001). Dust particles  
83 influence the earth’s radiation balance and supply micro-nutrients (e.g. iron) and macro-nutrients to the  
84 ocean surface waters (e.g. Jickells et al., 2005; Neuer et al., 2004). Additionally, dust acts as ballast mineral  
85 (Armstrong et al., 2002; Klaas and Archer, 2002) for organic carbon-rich particles (e.g. Fischer et al., 2009,

86 a, b; Bory and Newton, 2000; Iversen and Ploug, 2010; Iversen et al., 2010; Bressac et al., 2014). Dunne et  
87 al. (2007) suggested that dust may be the major carrier for organic carbon to the seafloor. A clear coupling  
88 between atmospheric dust occurrence and deep-sea lithogenic particle fluxes at 2000 m water depths was  
89 observed in the subtropical north Atlantic (33°N, 22°W; Brust et al., 2011). Fischer and Karakas (2009)  
90 proposed that high dust supply may increase particle settling rates by ballasting and result in relatively high  
91 organic carbon fluxes in the Canary Current system compared to other EBUEs. Wintertime African dust  
92 transport is suggested to be affected by the NAO (Chiapello et al. 2005; Hsu et al., 2012). As dust plays a  
93 major role in the Cape Blanc area with respect to deep ocean fluxes and the intensity of coastal upwelling is  
94 affected by the NAO as well, the major focus of this long-term study will be on the relationship between  
95 deep ocean mass fluxes and NAO forcing.

96 From the mesotrophic Cape Blanc study site  $CB_{\text{meso}}$  located about 200 nm off the coast (Fig. 1a), we  
97 obtained an almost continuous sediment trap record of fluxes (mostly from about 3500 m water depth) for  
98 the past 25 years (1988-2012, only interrupted between 1992 and 1993). Long time series of particle fluxes  
99 are rare, in particular from coastal upwelling sites with high productivity. Although SSTs and wind data  
100 analyses over longer time scales (e.g. decades) for the NW African upwelling system and other EBUEs are  
101 very important to test the ‘Bakun upwelling intensification hypothesis’ (Bakun, 1990; Cropper et al., 2014),  
102 any potential increase of upwelling intensity does not necessarily result in an increase of phytoplankton  
103 standing stock and/or productivity and/or deep ocean mass fluxes (e.g. Ducklow et al., 2009). Hence, for  
104 studying the potential changes of the biological pump and carbon sequestration in the deep ocean over  
105 decades and over a larger area, sediment traps are a primary and probably the best choice. As deep ocean  
106 sediment traps have a rather large catchment area for particles formed in the surface and subsurface waters  
107 (e.g. Siegel and Deuser, 1997), they integrate rather local and small-scale effects, events and processes in the  
108 highly dynamic EBUE off Mauritania.

109

## 110 **2. Study area**

### 111 ***2.1 Oceanographic and biological setting***

112 The sediment trap mooring array  $CB_{\text{meso}}$  is deployed in the Canary Current System within one of the four  
113 major EBUEs (Freon et al., 2009) (Fig. 1a). Coastal upwelling is driven there by alongshore trade winds,  
114 leading to offshore advection of surface waters, which are replaced by colder and nutrient-rich subsurface  
115 waters. Around 21°N off Cape Blanc, a prominent cold filament leads to offshore streaming of cold and  
116 nutrient-rich waters from the coast to the open ocean up to about 450 km offshore (Fig. 1a). This cold tongue  
117 is named the ‘giant Cape Blanc filament’ (Van Camp et al., 1991), being one of the largest filaments within  
118 all EBUEs.

119 The relationship between the coastal winds, SST and the biological response (e.g. changes in chlorophyll) off  
120 Mauritania seems to be strong and almost immediate (Mittelstaedt, 1991; Pradhan et al., 2006). Trade winds  
121 persist throughout the year and intensify in late winter to reach their highest intensity in spring (Barton et al.,

122 1998; Nykjaer and Van Camp, 1994; Meunier et al., 2012). According to Lathuilière et al. (2008), our study  
123 area is located within the Cape Blanc inter-gyre region (19-24°N) which is characterized by a weaker  
124 seasonality (peaks in winter-spring and fall). Following the definition by Cropper et al. (2014), our study  
125 area is situated on the southern rim of the strong and permanent coastal upwelling zone (21°-26°N) (Fig. 1a).

126 The cold and nutrient-rich southward flowing CC departs from the coastline south of Cape Blanc, later  
127 forming the North Equatorial Current (NEC) (Fig. 1a). South of about 20°N, a recirculation gyre drives a  
128 poleward coastal current fed by the North Equatorial Counter Current (NECC) during summer. The  
129 Mauritanian Current (MC) flows northward along the coast to about 20°N (Fig. 1a; Mittelstaedt, 1991),  
130 bringing warmer surface water masses from the equatorial realm into the study area. Where the CC departs  
131 from the coast, a NE-SW orientated salinity front in the subsurface waters is observed, the Cape Verde  
132 Frontal Zone (CVFZ, Zenk et al., 1991) (Fig. 1a), which separates the salty and nutrient-poor North Atlantic  
133 Central Water (NACW) from the nutrient-richer and cooler South Atlantic Central Water (SACW). Both  
134 water masses may be upwelled and mixed laterally and frontal eddies develop off Cape Blanc (Meunier et  
135 al., 2012) (Fig. 1a). Lathuilière et al. (2008) offered a comprehensive overview of the physical background,  
136 i.e. the ocean circulation off NW Africa.

137 Fig. 1.

138

## 139 ***2.2 Importance of dust supply and Sahel rain fall for the study area***

140 Dust supply from land to the low-latitude North Atlantic Ocean is not only dependent on the strength of the  
141 transporting wind systems (NE trade winds at lower levels and Saharan Air Layer above) but also on the  
142 rainfall and dryness in the multiple source regions in West Africa (Goudie and Middleton, 2001; Nicholson,  
143 2013). During long periods of droughts (e.g. in the 1980s), dust loadings over the Sahel experienced  
144 extraordinary increases (N'Tchayi Mbourou et al., 1997). As mass fluxes and settling rates of larger marine  
145 particles (i.e. marine snow) are assumed to be influenced by mineral dust particles via the ballasting effect  
146 (Armstrong et al., 2002; Fischer et al., 2009a, 2010; Iversen and Ploug, 2010; Bressac et al., 2014; Dunne et  
147 al., 2007; Thunell et al., 2007), climatic conditions on land need to be considered. The contribution of dust to  
148 the settling particles in the deep ocean off Cape Blanc amounts to one-third on average of the total mass flux  
149 (Fischer et al., 2010), but it may be as high as 50% during particular flux events (Nowald et al., 2015). As  
150 shown by Jickells et al. (2005), modelled dust fluxes from the Saharan region and their variability may be  
151 influenced by ENSO and NAO cycles (see also Goudie and Middleton, 2001; Chiapello et al., 2005; Hsu et  
152 al., 2012; Diatta and Fink, 2014). During the time period of this study (1988-2012, Fig. 2), the wintertime  
153 (Dec-Jan-Feb-Mar=DJFM) NAO index after Hurrell (Hurrell, 1995) is characterized by switches from  
154 extremely positive (e.g. 1989, 1990) to extremely negative values (e.g. in 1996, 2010) (Fig. 2).

155 Climate over West Africa is also influenced by the continental Inter-Tropical Convergence Zone (ITCZ; also  
156 named Intertropical Front, Nicholson, 2013). This low-pressure zone separates the warm and moist SW  
157 monsoon flow from the dry NE trade winds coming from the Sahara. The tropical rainbelt in the Atlantic

158 realm originates from the convergence of the NE and SE trade wind systems and migrates roughly between  
159  $\sim 3^{\circ}\text{S}$  (boreal winter) and  $\sim 15^{\circ}\text{N}$  (boreal summer) in the course of the year (Lucio et al., 2012). On longer  
160 timescales, severe Sahel drought intervals occurred in the 1980s (Chiapello et al., 2005; Nicholson, 2013).  
161 Recent evidence shows that Sahel rainfall may have recovered during the last two decades and that the  
162 region is now ‘greening’ (Fontaine et al., 2011; Lucio et al., 2012).

163 Fig. 2.

164

### 165 ***2.3 Large-scale teleconnections affecting the study area***

166 Ocean-atmosphere dynamics at our study site is influenced by large-scale atmospheric teleconnections and  
167 climate modes. Here, such teleconnections are illustrated based on results from a long-term present-day  
168 climate control run which was performed using the Comprehensive Climate System Model version 3  
169 (CCSM3; Collins et al., 2006; Yeager et al., 2006). Atmospheric sea-level pressure (SLP) patterns describe  
170 the near-surface air flow which affects ocean upwelling and currents as well. We therefore correlated  
171 simulated SLP with prominent teleconnection indices such as the NAO SLP index (Hurrell, 1995) and the  
172 Niño3 area-averaged ( $150^{\circ}\text{W}$ - $90^{\circ}\text{W}$ ,  $5^{\circ}\text{S}$ - $5^{\circ}\text{N}$ ) SST index, both calculated from the model results (Fig. 3).  
173 Boreal winter is the season where the NAO is strongest and where tropical Pacific SST anomalies associated  
174 with ENSO events tend to peak.

175 Correlations during winter show that NAO and ENSO may have opposite effects on the NW African/eastern  
176 Atlantic realm (Fig. 3 a,b), for instance on wind fields, and consequently on upwelling with potential  
177 implications for deep ocean mass fluxes. A positive phase of the NAO is associated with anomalous high  
178 pressure in the Azores high region (Fig. 3a) and stronger northeasterly winds along the NW African coast. In  
179 contrast, a positive phase of ENSO (El Niño event) goes along with a weakening of the northeasterlies in the  
180 study area (Fig. 3 b). It should be noted, however, that the magnitude of correlation in our study area is larger  
181 for the NAO than for ENSO. This should be taken into account when disentangling the relative importance  
182 of these climate modes. Apart from seasonal-to-interannual timescales, low-frequent climate variability may  
183 impact on our study area as well and is probably linked to Atlantic SST variations on decadal-to-interdecadal  
184 timescales, e.g. the Atlantic Multidecadal Oscillation (AMO). The correlation of SLP with area-averaged  
185 ( $0^{\circ}$ - $70^{\circ}\text{N}$ ,  $60^{\circ}$ - $10^{\circ}\text{W}$ ) SST fluctuations over periods above 10 years highlights a centre of action in the  
186 tropical Atlantic with SLP reductions (weaker northeasterly winds) along with higher Atlantic basin-wide  
187 SST during a positive AMO phase (Fig. 3c). This shows the potential importance of longer-term Atlantic  
188 basin-scale SST variations for alongshore winds and upwelling (trends) at our trap location

189 ENSO related teleconnections in the NW African upwelling system have been described by several authors  
190 (Behrenfeld et al., 2001; Pradhan et al., 2006; Zeeberg et al., 2008) and can be illustrated by the negative  
191 correlation of SLP with eastern tropical Pacific SST (Fig. 3b, chapter 3.3.). Fischer et al. (2009b) showed  
192 that the size of the Cape Blanc filament was small in winter-spring 1997-1998 and unusually high from fall  
193 1998 to spring 1999 (Fig. 7b; Fig. 1e). This is documented by reduced (warm El Niño) and elevated (cold La

194 Niña) deep ocean mass fluxes of all components. In certain years, the filament area was more than twice as  
 195 large in spring as in all (e.g. 1999 La Niña Event). Tropical Pacific variability on interannual ENSO  
 196 timescales is also an important factor in driving ecosystem variability in the California Current System (for a  
 197 summary see Checkley and Barth, 2009).

198 Fig. 3.

199

### 200 **3. Material and Methods**

#### 201 **3.1 Sediment traps and moorings**

202 We used deep-moored (>1000 m), large-aperture time-series sediment traps of the Kiel and Honjo type with  
 203 20 cups and 0.5 m<sup>2</sup> openings, equipped with a honeycomb baffle (Kremling et al., 1996). Mooring and  
 204 sampling dates are given in Table 1. As the traps were moored in deep waters (mostly below 1000m),  
 205 uncertainties with the trapping efficiency due to strong currents (e.g. undersampling, Yu et al., 2001;  
 206 Buesseler et al., 2007) and/or due to the migration and activity of zooplankton migrators ('swimmer  
 207 problem') are assumed to be minimal. Prior to the deployments, the sampling cups were poisoned with  
 208 HgCl<sub>2</sub> (1 ml of conc. HgCl<sub>2</sub> per 100ml of filtered seawater) and pure NaCl was used to increase the density  
 209 in the sampling cups to 40‰. Upon recovery, samples were stored at 4°C and wet-split in the home  
 210 laboratory using a rotating McLane wet splitter system. Larger swimmers such as crustaceans were picked  
 211 by hand with forceps and were removed by filtering carefully through a 1 mm sieve and all flux data here  
 212 refer to the size fraction of <1 mm. In almost all samples, the fraction of particles >1 mm was negligible,  
 213 only in a few samples larger pteropods were found.

#### 214 **3.2 Mass fluxes**

215 Analysis of the fraction < 1 mm, using ¼ or 1/5 wet splits, was performed according to Fischer and Wefer  
 216 (1991). Samples were freeze-dried and the homogenized samples were analyzed for bulk (total mass),  
 217 organic carbon, total nitrogen, carbonate and biogenic opal (BSi = biogenic silica). Organic carbon, nitrogen  
 218 and calcium carbonate were measured by combustion with a CHN-Analyser (HERAEUS). Organic carbon  
 219 was measured after removal of carbonate with 2 N HCl. Overall analytical precision based on internal lab  
 220 standards was better than 0.1% (±1σ). Carbonate was determined by subtracting organic carbon from total  
 221 carbon, the latter being measured by combustion without pre-treatment with 2N HCl. BSi was determined  
 222 with a sequential leaching technique with 1M NaOH at 85°C (Müller and Schneider, 1993). The precision of  
 223 the overall method based on replicate analyses is mostly between ±0.2 and ±0.4%, depending on the material  
 224 analyzed. For a detailed table of standard deviations for various samples we refer to Müller and Schneider  
 225 (1993). Lithogenic fluxes or the non-biogenic material was estimated according to:

$$226 \textit{lithogenic material} = \textit{dust} = \textit{total mass} - \textit{carbonate} - \textit{opal} - 2x\textit{C}_{org}$$

227

228 We estimated organic matter by multiplying organic carbon by a factor of two as about 50-60% of marine  
 229 organic matter is constituted by organic carbon (Hedges et al., 1992). Some studies have shown a clear linear

230 relationship between lithogenic fluxes and particulate aluminum (e.g. Ratmeyer et al., 1999a), the latter  
231 being derived from clay minerals as part of the lithogenic (non-biogenic) component. Grains size studies  
232 from Ratmeyer et al. (1999a, b) and further microscopic analysis provide evidence that most of the lithogenic  
233 material in the study area was derived from quartz grains in the fine silt fraction (10-30  $\mu\text{m}$ , see also Friese et  
234 al., 2016). Here we attribute the lithogenic flux to dust-derived material (=mineral dust flux) as no large  
235 rivers supply suspended material to the study area off Cape Blanc.

236 Due to logistical reasons, we had very different time resolutions of the sediment trap collections (a few days  
237 to several weeks) which limits comparisons between specific intervals and years. Seasonal fluxes were  
238 calculated and shown to allow comparison between the seasons mainly with respect to interannual  
239 variability. Seasons were defined using the dates of opening and closure of the sampling cups closest to the  
240 start of the astronomical seasons (March 21, June 21, September 23, December 21) (Table 2). Where lower  
241 trap data (around 3500 m) were not available, the upper trap data (around 1000 m) were used, which mostly  
242 match the lower trap fluxes with respect to seasonality (Fischer et al., 2009b). When plotting all available  
243 lower and upper trap total mass fluxes for winter, a close correspondence is observed ( $r^2=0.84$ ,  $N=10$ ), with  
244 slightly higher fluxes in the deeper trap due to lateral particle advection processes (Fischer et al., 2009b,  
245 Karakas et al., 2006, 2009). However, considering the entire record presented here, it seems that the upper  
246 trap fluxes of the winter seasons 1998 and 2004 may be critical due to smaller filament areas. As a  
247 consequence, the area/filament with elevated chlorophyll and high particle concentrations may not have  
248 reached the upper offshore trap. Because of lateral particle advection from the east (Karakas et al., 2006) and  
249 the larger catchment area of the deeper traps (Siegel and Deuser, 1997), particle fluxes might have been  
250 higher in the deeper water column in winter 1998 and 2004. In general, the seasonal patterns and the  
251 composition of the particle fluxes were rather similar between the upper and lower traps (Fischer et al.,  
252 2009b). The long-term means and standard deviations were calculated using only the available deeper trap  
253 flux values. The seasonal anomalies of the bulk fluxes were calculated using the deviations from the mean  
254 values of the respective seasons.

### 255 ***3.3 Carbonate producers***

256 To determine the major carbonate producers, the trap material was carefully wet-sieved with a 1 mm-screen  
257 and split into aliquots by a rotary liquid splitter. Generally a 1/5 split of the < 1 mm-fraction was used to pick  
258 planktonic foraminifers and pteropods from the wet solution. Foraminifers and pteropods were picked by  
259 hand with a pipette under a ZEISS Stemi 2000 microscope and rinsed with fresh water for three times and  
260 dried at 50°C overnight and counted. The mass fluxes of total carbonate producers expressed as  $\text{mg m}^{-2} \text{day}^{-1}$   
261 are mainly constituted of planktonic foraminifera, pteropods and nannofossils/coccolithophorids. Masses of  
262 foraminifera and pteropods were determined with a Sartorius BP 211D analytical balance.

### 263 ***3.4 Additional web-based data:***

264 To put our flux results from the deep ocean into a broader context, we used several observational datasets  
265 available from several the websites given below. For ocean colour, time series from the MODIS or SeaWiFS  
266 sensors based on a  $1^\circ \times 1^\circ$  box from  $20^\circ\text{N}$ - $21^\circ\text{N}$  and  $21^\circ$ - $20^\circ\text{W}$  (9 km resolution) slightly to the east of the



267 study site CB have been chosen due to the generally prevailing E-W directed current system, transporting  
 268 particles to the west (Helmke et al., 2005). Larger boxes, e.g. 2°x2° or 4°x4°, revealed similar results. For the  
 269 aerosol optical thickness (AOT, 869 nm, 9 km resolution), a 1°x1° box was chosen from the SeaWiFS and  
 270 MODIS data.

271 *Ocean colour from MODIS (9 km resolution):*

272 [http://oceancolor.gsfc.nasa.gov/cgi/l3?ctg=Standard&sen=A&prd=CHL\\_chlor\\_a&per=SN&date=21Jun2002&res=9km&num=24](http://oceancolor.gsfc.nasa.gov/cgi/l3?ctg=Standard&sen=A&prd=CHL_chlor_a&per=SN&date=21Jun2002&res=9km&num=24)

274 *Ocean colour from SeaWiFS (9 km resolution):*

275 [http://oceancolor.gsfc.nasa.gov/cgi/l3/S19972641997354.L3m\\_SNAU\\_CHL\\_chlor\\_a\\_9km.png?sub=img](http://oceancolor.gsfc.nasa.gov/cgi/l3/S19972641997354.L3m_SNAU_CHL_chlor_a_9km.png?sub=img)

276 *GIOVANNI-derived time series AOT (Aerosol Optical Thickness) and chlorophyll from SeaWiFS and  
 277 MODIS:*

278 [http://gdata1.sci.gsfc.nasa.gov/daac-bin/G3/gui.cgi?instance\\_id=ocean\\_month](http://gdata1.sci.gsfc.nasa.gov/daac-bin/G3/gui.cgi?instance_id=ocean_month)

279 *AOD (Aerosol Optical Depths) and dust and rainfall pattern (animation):*

280 [http://earthobservatory.nasa.gov/GlobalMaps/view.php?d1=MODAL2\\_M\\_AER\\_OD&d2=TRMM\\_3B43M](http://earthobservatory.nasa.gov/GlobalMaps/view.php?d1=MODAL2_M_AER_OD&d2=TRMM_3B43M)

281 *NAO (North Atlantic Oscillation) index based on station data of sea level pressure:*

282 <http://climatedataguide.ucar.edu/guidance/hurrell-north-atlantic-oscillation-nao-index-station-based>

283 *ENSO (El Niño-Southern Oscillation) Niño3.4 SST index:*

284 [http://iridl.ldeo.columbia.edu/filters/.NINO/SOURCES/.NOAA/.NCEP/.EMC/.CMB/.GLOBAL/.Reyn\\_SmithO](http://iridl.ldeo.columbia.edu/filters/.NINO/SOURCES/.NOAA/.NCEP/.EMC/.CMB/.GLOBAL/.Reyn_SmithO)  
 285 [Iv2/.monthly/.ssta/NINO34/T](http://iridl.ldeo.columbia.edu/filters/.NINO/SOURCES/.NOAA/.NCEP/.EMC/.CMB/.GLOBAL/.Reyn_SmithO)

286 *AMO (Atlantic Multidecadal Oscillation) SST index:*

287 <http://www.esrl.noaa.gov/psd/data/correlation/amon.us.data>

288 Table 1.

289

#### 290 **4. Results**

291 On the long-term, seasonal bulk fluxes were highest in boreal winter and summer and slightly lower in  
 292 spring and fall (Figs. 4, 5, 6a; Table 2). Total bulk fluxes reached 23.6 and 23.1 g m<sup>-2</sup> in winter and summer,  
 293 respectively (Table 2). For spring and fall, total mass fluxes were as high as 19.6 and 21.1 g m<sup>-2</sup>, respectively  
 294 (Table 2). However, the seasonal differences in the bulk fluxes are not statistically significant. Along with  
 295 the highest mass fluxes, winter and summer seasons also exhibit the highest standard deviations (Fig. 4),  
 296 pointing to a high interannual variability. In general, this interannual variability is clearly higher than the  
 297 seasonal differences in bulk fluxes. Only the lithogenic components, i.e. the mineral dust particles, did not  
 298 show an increase during summer and only peaked in winter (up to 7.4 g m<sup>-2</sup>) when dust plumes were most  
 299 frequent (Goudie and Middleton, 2001). High summer fluxes of up to 16.9 g m<sup>-2</sup> were mostly due to high  
 300 carbonate sedimentation (Fig. 4), both of primary (coccolithophores) and secondary producers (foraminifera  
 301 and pteropods). Organic carbon and BSi showed a rather similar pattern (Fig. 4, 6a) with a maximum in  
 302 winter (up to 1.1 and 1.7 g m<sup>-2</sup>, respectively) and a secondary maximum in summer/fall. This is reflected in  
 303 the close correspondence between both flux components for these seasons (Table 3). Highest mass fluxes

304 coinciding with highest positive flux anomalies lasting for several seasons occurred in 1988-89, 1998-99,  
305 and 2005-2006 (Fig. 5).

306 Following the strong ENSO cycle 1997-1999, total flux anomalies were low or negative over a longer period  
307 (fall 1999 to fall 2004), only interrupted by an episodic peak in summer 2002 (Fig. 5a, b). Other episodic  
308 peaks in sedimentation were found in winter/spring 1996-1997 and in the winter seasons 2004-2005, 2006-  
309 2007 and 2009-2010 (Fig. 5a, b). Longer intervals (several seasons) of negative flux anomalies were  
310 obtained in 1997-98 and 2009-11 (Fig. 5b). Total fluxes decreased from 1988 to 1991, from spring 2007 to  
311 2010, later increasing from 2010 to 2012 (Fig. 5).

312 In general, the major bulk flux components followed the total flux and were well inter-correlated, except that  
313 the relationship between organic carbon and carbonate was weak in summer (Table 3). However, the  
314 regression-based relationships (i.e. the slope) varied interannually (e.g. Fischer et al., 2009a). The matrix in  
315 Table 3 shows the correlation coefficients between organic carbon and nitrogen, BSi, carbonate and  
316 lithogenic fluxes for the four seasons (lower traps only). Organic carbon and BSi (mainly diatoms) were  
317 highly correlated during the major upwelling events in winter ( $R^2=0.70$ ) and summer/fall, whereas the  
318 relationship between organic carbon and total carbonate in summer was weak ( $R^2=0.16$ , Table 3). Dust  
319 fluxes peaked together with organic carbon, preferentially in winter and fall ( $R^2=0.63$  and  $0.67$ , respectively  
320 Table 3). The tight coupling between organic carbon and nitrogen is not surprising as both elements  
321 constitute organic matter formed during photosynthesis, which is later degraded in the upper water column  
322 forming sinking phytodetritus. The slope is almost constant (0.13-0.11) and the reciprocal value reflects the  
323 Redfield Ratio (Redfield et al., 1963) of the sinking organic-rich particles (Table 3). The molar C:N varied  
324 seasonally between 8.9 and 10.6, typical for sinking detritus collected in deep sediment traps.

325 On the long-term, the composition of settling particles in the deeper traps off Cape Blanc consisted of  
326 roughly 57% carbonate, ca. 30% lithogenic particles, 4% organic carbon, 0.5% nitrogen and 5% BSi (Fig. 4).  
327 BSi contained mostly a mixture of coastal and open-ocean diatoms (Romero et al. 1999, 2002, and unpubl.  
328 data). The BSi flux pattern (Fig. 6) was influenced by switches from a positive to a negative NAO index  
329 which were reflected in decreasing winter opal fluxes, e.g. from 1989 to 1991, 1995-1996 and 2007 to 2010.  
330 From 2001 through 2006, NAO variability was rather low and the index was around zero or slightly negative  
331 (Fig. 6c; Table 4). Nevertheless, BSi fluxes varied considerably and showed episodic peaks in the summer  
332 seasons 2001, 2002 and 2003 (Fig. 6a, b), BSi flux was high and showed positive anomalies in 2005, except  
333 for spring 2005 (Fig. 6a, b; Table 4).

334 The general flux pattern of BSi (Fig. 6a, b) with values from almost zero to  $1.91 \text{ g m}^{-2}$  did not match the  
335 SeaWiFS ocean colour time series trend which showed an overall decrease in chlorophyll from 1997 to 2010  
336 (Fig. 6d). The organic carbon flux pattern (not shown, values from almost zero to  $1.1 \text{ g m}^{-2}$ ) did not follow  
337 the ocean colour data from MODIS/SeaWiFS either. Peak chlorophyll values were observed mostly during  
338 spring, except in 1998 (fall maximum) and 2007 (summer maximum). The MODIS ocean colour values  
339 generally mimicked the SeaWiFS pattern, except for the discrepancy in summer 2010 (Fig. 6d).

340 Tables 2-3; Figs. 4-6.

## 341 **5. Discussion**

### 342 **5.1 Particle transport processes in the water column**

343 Mass fluxes and particle transport processes off Cape Blanc (Mauritania) have been described by  
344 summarizing articles of Fischer et al. (2009b) and Karakas et al. (2006). Common flux patterns were the  
345 increase of fluxes in late winter-spring and late summer of all components at both trap levels. This matched  
346 the seasonal intensification of coastal upwelling (e.g. Meunier et al., 2012) due to wind forcing and a  
347 stronger offshore streaming of the Cape Blanc filament (e.g. Fischer et al., 2009b). The increase of fluxes in  
348 late summer to fall was mostly due to enhanced biogenic carbonate sedimentation (Fig. 4e), associated with  
349 the northward flowing warm MC, coming from tropical regions (Mittelstaedt, 1991). In the Canary Current  
350 upwelling system, which is dominated by carbonate producers, particle settling rates are rather high (around  
351  $300 \text{ m d}^{-1}$ ), compared to EBUEs dominated by BSi sedimentation (Fischer and Karakas, 2009; Fischer et al.,  
352 2009a). As suggested by Fischer et al. (2009a), the relatively high organic carbon flux in the deep ocean off  
353 NW Africa may be due to the high availability of mineral ballast, i.e. from coccolithophorids and fine-  
354 grained mineral dust (Iversen et al., 2010; Iversen and Ploug, 2010; Ploug et al., 2008). Direct evidence for  
355 the influence of the deposition of dust particles on the settling rates of larger particles and the flux  
356 attenuation in the epi- and mesopelagic has been found on short timescales, i.e. days. This was observed  
357 during a severe dust outbreak in January 2012 (Iversen, unpubl. observations) by deploying drifting traps  
358 before and after the dust outbreak (Fig. 8a, insert image).

### 359 **5.2 Influence of the NAO on biogenic silica sedimentation**

360 The NAO both affects coastal upwelling and productivity off Mauritania through wind forcing (upwelling)  
361 and dust/nutrient supply (Chiapello et al., 2005), mainly during winter (DJFM) (Goudie and Middleton,  
362 2001; Cropper et al., 2014). Indeed, we observed an increase of both the winter NAO index and associated  
363 winter BSi fluxes (Fig. 6, 7a), the latter known to be indicative of coastal upwelling strength and  
364 productivity. When plotting winter BSi fluxes versus the Azores pressure alone (DJFM Ponta Delgada SLP,  
365 1989-2002), the relationship improves slightly ( $R^2=0.19$   $N=11$ , not shown) but remains statistically  
366 insignificant. Since upwelling is wind-driven and large-scale wind patterns in the study area are positively  
367 correlated to NAO variability (Fig. 3a), a close linkage between a positive (negative) NAO and higher  
368 (lower) BSi fluxes can be expected. Organic carbon flux showed less correspondence to the winter NAO  
369 index (not shown). No clear relationship can be seen between the winter (DJFM) NAO index and BSi and  
370 organic carbon fluxes later in spring, if we consider a time delay of a few weeks between wind forcing of  
371 coastal upwelling, high chlorophyll standing stock, particle formation and sedimentation and, finally, the  
372 documentation of increasing fluxes in the deep traps in spring.

373 From 2001 to 2006 when the winter NAO index became close to zero (Fig. 6c), the BSi flux showed rather  
374 unusual (episodic) peaks either in summer, fall or in winter 2004-2005 (Fig. 6a, b). This suggests increasing  
375 coastal upwelling in summer and fall (e.g. Cropper et al., 2014) and/or a strengthening of the northward  
376 flowing and warmer MC, combined with an enhanced supply of a nutrient- and Si-rich source water  
377 (SACW instead of NACW). We favour the latter scenario as there is evidence of unusual warm surface water

378 conditions (SST anomalies of +3°C) related to weak trade wind intensity between 2002 and 2004 (Zeeberg et  
 379 al., 2008, Alheit et al., 2014). These conditions might have led to a stronger influence of the northward  
 380 flowing MC and the silicate-richer SACW which mixes into the Cape Blanc upwelling filament and, thus,  
 381 contributed to higher BSi productivity and sedimentation. Such a scenario was proposed by Romero et al.  
 382 (2008) to explain the extraordinary high content of BSi in Late Quaternary sediments deposited off Cape  
 383 Blanc during Heinrich Event 1 and Younger Dryas following the Last Glacial Maximum.

384 The 2004-2005 winter BSi flux clearly falls off the regression line of winter BSi flux versus the winter NAO  
 385 index (Fig. 7a). Exceptional conditions in 2005 are also indicated when plotting the area with high  
 386 chlorophyll ( $> 1 \text{ mg Chla m}^{-3}$ ) covered by the Cape Blanc filament (Fischer et al., 2009) versus the BSi  
 387 fluxes (Fig. 7b). In general, a larger (smaller) Cape Blanc filament area has been associated with higher  
 388 (lower) BSi fluxes (Fig. 7b) and also with higher total mass fluxes (not shown). However, in winter of 2004-  
 389 2005 (a relatively cold season with negative SST anomalies), the filament area was smaller and chlorophyll  
 390 standing stock was lower (Fig. 6d, 7b). Nevertheless, BSi fluxes were the highest of the entire record. The  
 391 seasonal variability of chlorophyll from the entire SeaWiFS record (1997-2010, Fig. 6d) indicates no  
 392 relationship between the chlorophyll standing stock and deep ocean BSi flux (or organic carbon flux, not  
 393 shown). These observations point to additional regulators for organic carbon and BSi export to the deep sea.  
 394 Ocean colour imagery even revealed a decreasing trend from 1997 to 2010 (Fig. 6d), which suggests a  
 395 decrease in upwelling. This is not consistent with the ‘Bakun upwelling intensification hypothesis’ (Bakun,  
 396 1990) nor with studies from Kahru and Mitchell (2008). Throughout 2005, however, the positive BSi flux  
 397 anomalies corresponded well with positive dust flux anomalies (Fig. 6b, 8b). As seen from Aerosol Optical  
 398 Thickness (AOT, Fig. 8c), dust availability was rather high in 2005 and corresponded to high dust  
 399 sedimentation in summer and fall 2005 (Fig. 8; see chapter 5.3). We suggest, therefore, that the linear  
 400 relationship between the NAO index and BSi fluxes may be biased in years of anomalous dust input into the  
 401 surface ocean.

402 Fig. 7.

403

### 404 ***5.3 Interaction between mineral dust and the biological pump***

405 Fischer and Karakas (2009) stated that particle settling rates and organic carbon fluxes in the Canary Current  
 406 system were unusually high compared to other EBUEs. This was mainly attributed to particle loading by dust  
 407 particles (see also Fischer et al., 2009a, b, Iversen et al., 2010). BSi and lithogenic (mineral dust) fluxes point  
 408 to a close linear relationship ( $R^2=0.78$ ,  $N=21$ , Fig. 9a) mainly in winter where dust availability and  
 409 deposition is high (Goudie and Middleton, 2001), but not in summer ( $R^2=0.56$ ,  $N=23$ , Fig. 9b). High supply  
 410 of dust into the surface ocean is often associated with dry conditions in the Sahel/Sahara in the previous year  
 411 (Engelstaedter et al., 2006; Prospero and Lamb, 2003; Moulin and Chiapello, 2004). Indeed, the interval  
 412 2002-2004 in particular is known to have been much warmer and drier during summer/autumn on land and in  
 413 the ocean (Zeeberg et al., 2008; Alheit et al., 2014). These conditions might have allowed the later wind-

414 induced mobilization of larger amounts of dust particles into the atmosphere and led to a dust-enriched  
415 atmosphere during the entire year 2005, combined with elevated deep ocean mass fluxes.

416 Typically, highest dust flux off Cape Blanc occurs in winter, whereas part of the summer dust load (Fig. 8) is  
417 transported further westward and deposited in the Caribbean Sea (Goudie and Middleton, 2001; Prospero and  
418 Lamb, 2003). However, the rainfall pattern exhibits elevated precipitation in summer and fall 2005 when the  
419 tropical rainbelt was far north; this might have led to unusual wet deposition of dust in summer over our  
420 study site (Friese et al., 2016). As shown earlier, BSi fluxes show positive anomalies in summer and fall  
421 2005 (Fig. 6b), pointing to a stronger dust-influenced biological pump.

422 In contrast to BSi, winter sedimentation of mineral dust did not show any common trend with the winter  
423 NAO index (not shown). Using satellite-derived AOT, Chiapello et al. (2005) suggested a close relationship  
424 of atmospheric dust content and the NAO index. High AOT, however, does not necessarily correspond with  
425 high dust deposition into the ocean. Moreover, dust deposition into the ocean surface does not unavoidably  
426 and directly result in particle export and transfer to the deep ocean. Dust deposition is not only controlled by  
427 wind strength and direction in the trap area but also by source region conditions and precipitation over the  
428 trap site. Consequently, considering the NAO as the only controlling factor for dust deposition and  
429 sedimentation even if the correlation between SLP (and thus winds) and NAO is strong in the study area  
430 (Fig. 3a), would be an oversimplification.

431 Another explanation for the missing relationship could be that fine-grained dust accumulates in surface  
432 waters until the biological pump produces sufficient organic particles to allow the formation of larger  
433 particles which then settle into the deep ocean (Bory et al., 2002; Ternon et al., 2010, Nowald et al., 2015).  
434 Cape Blanc dust particles have predominant grain sizes between 10 and 20  $\mu\text{m}$  (Ratmeyer et al., 1999a, b;  
435 Friese et al., 2016) and, thus, would sink too slowly to build a deep ocean flux signal. We propose that only  
436 the close coupling between the organic carbon pump, dust particles and the formation of dense and larger  
437 particles led to elevated export and sedimentation (Bory et al., 2002; Fischer et al., 2009a, Fischer and  
438 Karakas, 2009). Thunell et al. (2007) found that organic carbon fluxes strongly correlated with mineral  
439 fluxes in other upwelling-dominated continental margin time series such as the Santa Barbara Basin located  
440 within the California Current System. However, the detailed processes and interaction between different  
441 groups of phytoplankton and types of ballast minerals (e.g. quartz versus clay minerals etc.) are largely  
442 unknown and need clarification. Laboratory experiments with different ballast minerals (e.g. Iversen and  
443 Roberts, 2015) and measurements of organic carbon respiration and particle settling rates suggest a  
444 significant influence of ballast minerals on particle settling rates, carbon respiration and flux (Ploug et al.,  
445 2008; Iversen and Ploug, 2010). In a time series study with optical measurements, addressing particle  
446 characteristics (e.g. sizes) and using fluxes at the nearby eutrophic sediment trap off Cape Blanc ( $\text{CB}_{\text{eu}}$ ),  
447 Nowald et al. (2015) suggested an influence of dust outbreaks on particle sedimentation down to 1200 m.  
448 Interestingly, settling organic-rich particles off Cape Blanc were only around 1 mm in size during the two-  
449 year deployment from 2008 to 2010 (Nowald et al., 2015). Higher fluxes were mostly attributed to higher

450 numbers of small particles rather than to larger particle sizes during blooms in the Cape Blanc area (Nowald  
451 et al., 2015).

452 Figs. 8, 9.

453

#### 454 **5.4 Carbonate fluxes and potential ENSO teleconnections**

455 Deep ocean total mass and carbonate fluxes (Figs. 5 and 10) showed elevated values over more than a year  
456 from summer 1998 to fall 1999 during a La Niña event, whereas BSi and dust fluxes showed positive  
457 anomalies of shorter duration (fall 1998 to spring 1999) (Fig. 6b). Investigating SeaWiFS-derived ocean  
458 colour in the Mauritanian upwelling region, Pradhan et al. (2006) obtained a link between the multivariate  
459 ENSO index, the strength of upwelling and the chlorophyll standing stock (250% increase) during the 1998-  
460 1999 La Niña. They also observed that during the mature La Niña phase in the Pacific Ocean, NW African  
461 trade winds increased in winter-spring. Coincidentally, Helmke et al. (2005) obtained a more than doubling  
462 of the deep ocean organic carbon fluxes in fall 1998 to summer 1999 during the major La Niña phase.

463 We obtained positive carbonate flux anomalies with a longer duration in summer 1998 to fall 1999 and  
464 summer 2005 to spring 2006 (Fig. 10b). During fall 1998 (La Niña phase), the area of the Cape Blanc  
465 filament was unusually large compared with fall 1997 (El Niño phase) (Fig. 1 d, e). The contribution of  
466 major carbonate producers to total carbonate flux varied both on seasonal and interannual timescales (Fischer  
467 et al., 2009a). These authors observed that nannofossils contributed almost 95% to carbonate sedimentation  
468 in 1991 (a relatively cold year) but only 64% in 1989 (a relatively warm year). On the long-term,  
469 nannofossils showed a rather low seasonality. Among the calcareous microorganisms, pteropods had the  
470 strongest seasonal signal which did not quite match the pattern of carbonate flux (Fig. 10a, c). As previously  
471 observed by Kalberer et al. (1993), a possible explanation is the high pteropod flux (mostly *Limacina inflata*)  
472 in summer 1989 due to unusual high SSTs. In our record, we found distinct pulses of pteropods in the  
473 summer seasons of 1998, 2002 and 2004 (Fig. 10c). In particular, the peaks in 2002 and 2004 can be  
474 attributed to anomalously warm conditions in the study area (Zeeberg et al., 2008; Alheit et al., 2014). Here,  
475 a period of near-neutral NAO together with an almost permanent El Niño phase during 2002-2004  
476 might have acted in concert towards weakening trade winds which allows a stronger influence of  
477 the warm and northward flowing MC, supplying high amounts of pteropods from tropical waters. In  
478 summary, ENSO may impact differently on different flux components. Whereas an increase in  
479 pteropod fluxes is found during the El Niño phase, La Niña induces an increase in total carbonate  
480 flux.

481 Fig. 10.

482

483

## 484 *5.5 Decadal variability and potential trends in mass fluxes*

485 Our records allow a first estimate of deep-ocean mass flux variations beyond seasonal-to-interannual  
486 timescales. The ‘Bakun upwelling intensification hypothesis’ (Bakun, 1990) has been supported by other  
487 studies using long-term SSTs, wind stress records or upwelling indices (e.g. Cropper et al., 2014, Narayan et  
488 al., 2010). Kahru and Mitchell (2008) applied satellite derived chlorophyll time series from SeaWiFS to  
489 conclude that chlorophyll standing stock in major upwelling regions of the world oceans had increased since  
490 September 1997. However, these records are rather short (1997-2006) and started in an unusual period with  
491 the strongest ENSO ever reported (1997-1998). In our record, no long-term trend in any mass flux  
492 component from 1988 through 2012 is seen, which indicates a long term increase or decrease in the strength  
493 of coastal upwelling off Cape Blanc. The 1997-2010 chlorophyll time series from SeaWiFS (Fig. 6d) shows  
494 a decreasing standing stock, which might indicate a decrease in the strength of coastal upwelling in the Cape  
495 Blanc area. The upwelling indices used by Cropper et al. (2014) showed a decreasing trend from 1980 to  
496 2013 for the Mauritanian-Senegalese upwelling zone (12-19°N), while observing some interdecadal  
497 variability. All these observations together point to regional differences within the upwelling system along  
498 the NW African coast (Cropper et al., 2014) with respect to long-term trends in upwelling and chlorophyll  
499 standing stock. According to these findings, only the southernmost weak permanent upwelling zone (21-  
500 26°N) would be in concert with the ‘Bakun upwelling intensification hypothesis’. Another implication is that  
501 trends detected from near-surface data/indices are not necessarily reflected in changes of deep-ocean mass  
502 fluxes and organic carbon sequestration. No evidence of decreasing dust fluxes from the Sahara/Sahel is seen  
503 in our lithogenic (dust) flux record (Fig. 8a), which might indicate ‘Saharan greening’ and reduced dust  
504 plumes during the past two decades (Zhao et al., 2010; Fontaine et al. 2011). Thus, mass flux patterns might  
505 be partly independent from chlorophyll standing stock or the size of the Cape Blanc filament.

506 Long-term model simulations under present-climate boundary conditions allow to study the  
507 linkages within the climate system on decadal timescales and beyond. Climate modes such as the  
508 AMO are operating in this frequency band, and a correlation between large-scale patterns of SLP  
509 and North Atlantic SST (AMO) index (both lowpass-filtered for periods above 10 years, Fig. 3c)  
510 suggests that even on these long timescales, climate modes such as the AMO might impact on  
511 climate variables such as SLP, SST and wind patterns, specifically through a weakening of the trade  
512 winds over the eastern Atlantic during the AMO warm phase (Fig. 3c). This response of the winds  
513 to low-frequent SST variations is consistent with earlier findings on interdecadal Atlantic SST  
514 variability (Kushnir, 1994; Alexander et al., 2014), and could influence the main characteristics of  
515 particle fluxes at our study site (Fig. 5). However, as current particle flux records from sediment  
516 traps only cover a few decades and cannot resolve AMO cycles with statistical robustness,  
517 continuation of trap experiments are essential to capture all relevant timescale variations. They will  
518 help to understand modern particle settling rates and the interpretation of marine sediment records  
519 used in paleoclimate reconstructions.

## 520 **6. Summary and Conclusions**

521 In our study, we presented a sediment trap record from the Eastern Boundary Upwelling Ecosystem area off  
522 Cape Blanc (Mauritania) for the period 1988-2012. Our major findings can be summarized as follows (also  
523 see Table 4):

524 1. Winter BSi fluxes showed a trend of increasing values with an increasing NAO Hurrell Index and the  
525 increasing Azores SLP as well. However, both relationships are statistically insignificant.

526 2. Episodic BSi flux peaks occurred between 2000 and 2005 when the NAO was neutral or negative. Dust  
527 outbreaks, followed by dry (winter) and wet (summer) deposition (e.g. in 2005) into the ocean, might have  
528 modified the efficiency of the biological pump and resulted in increased downward fluxes (e.g. of BSi or  
529 organic carbon) which were not related to any large scale forcings

530 3. Only the extreme 1997-2000 ENSO was documented clearly in the record, with low fluxes for almost a  
531 year during the warm El Niño phase, followed by high fluxes of almost a year during the following cold La  
532 Niña phase.

533 4. In addition to episodic BSi fluxes, episodic peaks of pteropods occurred in the summers 2002 and 2004  
534 (Fig. 10c, Table 4). This occurred during a neutral NAO phase and weakening trade winds, allowing a  
535 stronger influence from tropical surface waters from the south via the Mauritanian Current (MC) and an  
536 entrainment of Si-rich subsurface waters.

537 5. Teleconnections from ENSO and the NAO may have opposite effects on the NW African  
538 upwelling (Fig. 3) with potential implications for deep ocean mass fluxes. In particular, ENSO  
539 might confound the relationship between the NAO and BSi fluxes.

540 6. Fluxes from 1988 to 2012 point to a long-term decadal variability, probably related to the Atlantic  
541 Multidecadal Oscillation. However, the time series record is too short to reproduce AMO cycles with  
542 statistical robustness.

543 7. No long-term trend of any flux component was observed in the Mauritanian upwelling off Cape Blanc and  
544 therefore does not support the ‘Bakun upwelling intensification hypothesis’ (Bakun, 1990; Cropper et al.,  
545 2014).

546 8. We found no evidence of an increasing/decreasing supply of dust and its deposition off Mauritania  
547 between 1988 and 2012.

548 Table 4.

549

550 The long-term flux record allows insights into the influences of major climatic oscillations such as the NAO  
551 and on particle export and transfer of particles to the deep ocean and might help to evaluate how the  
552 ecosystem off Mauritania could develop in the future. We have some indications that the relationships  
553 between major Northern Hemisphere climate oscillations (e.g. the NAO) and deep ocean mass fluxes are



554 weakened by short-term ecosystem perturbations, e.g. due to dust outbreaks, the latter probably leading to  
555 episodic sedimentation pulses into the deep ocean. The complex processes of the interaction of non-biogenic  
556 particles (e.g. different minerals within dust, e.g. Iversen and Roberts, 2015) with organic materials produced  
557 by photosynthesis, aggregate formation and disintegration in the epi- and mesopelagic, particle  
558 characteristics (e.g. Nowald et al., 2015), settling rates and remineralization require further process studies,  
559 combined with laboratory experiments and different modelling approaches (e.g. particle (dis-) aggregation,  
560 Karakas et al., 2009).

561 Additionally, our record provides information on potential long-term changes or trends of mass fluxes which  
562 point to ecosystem changes or an intensification/weakening of the NW African upwelling system in the study  
563 area. Considering the present record of bulk fluxes of more than two decades, we have no indication of any  
564 long-term trend which might suggest a fundamental ecosystem change or a regime shift (step-wise change)  
565 in this important coastal upwelling ecosystem.

566

#### 567 *Author contribution*

568 G. Fischer prepared the ms with contributions from the co-authors. O. Romero investigated the diatom  
569 producers and contributed to the discussion, U. Merkel contributed the model simulations and the analysis,  
570 B. Donner studied the carbonate producers, M. Iversen and his group did the dust experiments and provided  
571 unpublished results/observations, N. Nowald and V. Ratmeyer performed the optical observations and  
572 analysis of particles, G. Ruhland and M. Klann designed the sediment trap experiments and analysed the  
573 sediment trap samples, G. Wefer planned the entire program and contributed to the discussion.

574

#### 575 *Acknowledgements*

576 We are greatly indebted to the masters and crews of many expeditions (Table 2). Many thanks also go to the  
577 chief scientists of the expeditions for their support during the cruises and for the planning activities and  
578 cooperations. We also would like to thank the Mauritanian, Moroccan and German authorities for their help  
579 during the planning phases of the expeditions. This work was only possible because of the long-term funding  
580 by the Deutsche Forschungsgemeinschaft through the SFB 261 (The South Atlantic in the Late Quaternary:  
581 Reconstruction of Mass Budget and Current Systems, 1989-2001) and the Research Center Ocean Margins.  
582 During about the last decade, the study is supported by the Marum Excellence Cluster, ‘The Ocean in the  
583 Earth System’. The model simulation done by U. Merkel has been performed at the supercomputer of the  
584 Norddeutscher Verbund für Hoch- und Höchstleistungsrechnen (HLRN), Hannover, Germany. We thank the  
585 two anonymous reviewers for helpful, fair and constructive comments and the associate editor for handling  
586 the manuscript.

587

588

589 **References**

- 590 Alexander, M.A., Kilbourne, K.H., and Nye, J.A.: Climate variability during warm and cold phases of the  
591 Atlantic Multidecadal Oscillation (AMO) 1871–2008. *J. Marine Syst.*, Vol. 133, 14-26, 2014.
- 592 Alheit, J., Licandro, P., Coombs, S., Garcia, A., Giráldez, A., Santamaría, M.T.G., Slotte, A. and Tsikliras,  
593 A.C.: Atlantic Multidecadal Oscillation (AMO) modulates dynamics of small pelagic fishes and  
594 ecosystem regime shifts in the eastern North and Central Atlantic. *J. Marine Syst.*, 133, 88-102, 2014.
- 595 Aristegui, J., Barton, E. C., Álvarez-Salgado, X. A., Santos, A. M. P., Figueiras, F. G., Kifani, S.,  
596 Hernández-León, S., Mason, E., Machú, E., and Demarcq, H.: Sub-regional ecosystem variability in the  
597 Canary Current upwelling, *Prog. Oceanogr.*, 83, 33–48., 2009.
- 598 Armstrong, R.A., Lee, C., Hedges, J.I., Honjo, S., and Wakeham, S.G.: A new mechanistic model of organic  
599 carbon fluxes in the ocean based on the quantitative association of POC with ballast minerals, *Deep-Sea*  
600 *Res. II*, 49, 219-236, 2002.
- 601 Bakun, A.: Global climate change and intensification of coastal ocean upwelling. *Science* 247, 198-201,  
602 1990.
- 603 Barton, E. D., Aristegui, J., Tett, P., Cantón, M., García-Braun, J., Hernández-León, S., Nykjaer, L.,  
604 Almeida, C., Almunia, J., Ballesteros, S., Basterretxea, G., Escánez, J., García-Weill, L., Hernández-  
605 Guerra, A., López-Laatzén, F., Molina, P., Montero, M.F., Navarro-Pérez, E., Rodríguez, J. M., van  
606 Lenning, K., Vélez, H., and Wild, K.: Eastern Boundary of the North Atlantic: northwest Africa and  
607 Iberia, in: *The Global Coastal Ocean*, Vol. 11, edited by: Robinson, A. R. and Brink, K., John Wiley and  
608 Sons, New York, Chichester, Weinheim, Brisbane, Singapore, Toronto, 29–67, 1998.
- 609 Behrenfeld, M. J., Randerson, J. T., McClain, C. R., Feldman, G. C., Los, S. O., Tucker, C. J., Falkowski, P.,  
610 Field, C. B., Frouin, R., Esaias, W. E., Kolber, D. D., and Pollack, N. H.: Biospheric primary production  
611 during an ENSO transition, *Science*, 291, 2594–2597, 2001.
- 612 Behrenfeld, M.J., and Falkowski, P.G.: Photosynthetic rates derived from satellite based chlorophyll  
613 concentration. *Limnol. Oceanogr.*, 42 (1), 1–20, 1997.
- 614 Bode, A., Alvarez-Ossorio, M.T., Cabanas, J.M., Miranda, A., and Varela, M.: Recent trends in plankton and  
615 upwelling intensity off Galicia (NW Spain). *Prog. Oceanogr.*, 83, 1-4, 342-350, 2009.
- 616 Bory, A.J.M., and Newton, P.P.: Transport of airborne lithogenic material down through the water column in  
617 two contrasting regions of the eastern subtropical North Atlantic Ocean. *Global Biogeochem. Cycles* 14  
618 (1), 297–315, 2000.
- 619 Bory, A., Dulac, F., Moulin, C., Chiapello, I., Newton, P.P., Guelle, W., Lambert, C.E., and Bergametti, G.:  
620 Atmospheric and oceanic dust fluxes in the northeastern tropical Atlantic ocean: how close a coupling?  
621 *Ann. Geophys.*, 20, 2067–2076, 2002.
- 622 Bressac, M., Gieu, C., Doraxan, D., Bourrin, F., Desboeufs, K., Leblond, N., and C. Ridame: Quantification  
623 of the lithogenic pump following a dust deposition event, *Biogeosciences*, 11, 1007-1020, 2014.
- 624 Brust, J., Schulz-Bull, D.E., Leipe, T., Chavagnac, V., and Waniek, J.J.: Descending particles: from the  
625 atmosphere to the deep ocean: A time series study in the subtropical NE Atlantic. *Geophys. Res. Lett.*, 38,  
626 L06603. <http://dx.doi.org/10.1029/2010GL045399>, 2011.
- 627 Buesseler, K. O., Antia, A. A., Chen, M., Fowler, S. W., Gardner, W. D., Gustafsson, O., Harada, K.,  
628 Michaels, A. F., Rutgers van der Loeff, M., Sarin, M., Steinberg, D. K., and Trull, T.: An assessment of  
629 the use of sediment traps for estimating upper ocean particle fluxes, *J. Mar. Res.*, 65, 345–416, 2007.
- 630 Carr, M.-E.: Estimation of potential productivity in Eastern Boundary Currents using remote sensing. *Deep-*  
631 *Sea Res. I*, 49, 59–80, 2002.
- 632 Checkley, D.M.Jr., and Barth, J.A.: Patterns and processes in the California Current Systems. *Prog.*  
633 *Oceanogr.*, 83, 49-64, 2009.
- 634 Chiapello, I., Moulin, C., and Prospero, J.M.: Understanding the long-term variability of African dust  
635 transport across the Atlantic as recorded in both Barbados surface concentrations and large-scale Total  
636 Ozone Mapping Spectrometer (TOMS) optical thickness. *J. Geophys. Res.*, 110, D18S10,  
637 doi:10.1029/2004JD005132, 2005.

- 638 Collins, W. D., Bitz, C.M., Blackmon, M.L. Bonan, G.B., Bretherton, C.S., Carton, J.A., Chang, P., Doney,  
639 S.C., Hack, J.J., Henderson, T.B., Kiehl, J.T., Large, W.G., McKenna, D.S., Santer, B.D., and Smith,  
640 R.D.: The Community Climate System Model Version (CCSM3), *J. Climate*, 19, 2122-2143. 2006.
- 641 Cropper, T.E., Hanna, and E., Bigg, G.R.: Spatial and temporal seasonal trends in coastal upwelling off  
642 Northwest Africa, 1981–2012. *Deep-Sea Res. II*, 86, 94–111, 2014.
- 643 Diatta, S., and Fink, A. H.: Statistical relationship between remote climate indices and West African  
644 monsoon variability, *Int. J. Climatol.*, 34, 3348–3367, doi:10.1002/joc.3912, 2014.
- 645 Ducklow, H.W., Doney, S.C., and Steinberg, D.K.: Contributions of long-term research and teim-sereis  
646 observations to marine ecology and biogeochemistry. *Annu. Rev. Mar. Sci.*, 1, 279-302, 2009.
- 647 Dunne, J. P., Sarmiento, J.L., and Gnanadesikan, A.: A synthesis of global particle export from the surface  
648 ocean and cycling through the ocean interior and on the seafloor, *Global Biogeochem. Cycles*, 21,  
649 GB4006, doi:10.1029/2006GB002907, 2007.
- 650 Engelstaedter, S., Tegen I., and Washington, R.: North African dust emissions and transport. *Earth Sci. Rev.*,  
651 79, 73-100, 2006.
- 652 Fischer, G., and Wefer, G.: Sampling, preparation and analysis of marine particulate matter. In: *The Analysis  
653 and Characterization of Marine Particles*, edited by Hurd, D.C., and Spencer, D.W., *Geophysical  
654 Monograph Series*, No. 63, 391-397, 1991.
- 655 Fischer, G., Donner, B., Ratmeyer, V., Davenport, R., and Wefer, G.: Distinct year-to-year particle flux  
656 variations off Cape Blanc during 1988–1991: Relation to delta  $\delta^{18}\text{O}$ -deduced sea-surface temperatures  
657 and trade winds. *J. Marine Res.*, 54 (1), 73–98, 1996.
- 658 Fischer, G., Wefer, G., Romero, O., Dittert, N., Ratmeyer, V. and Donner, B.: Transfer of particles into the  
659 deep Atlantic and the global Ocean: control of nutrient supply and ballast production. In: *The South  
660 Atlantic in the Late Quaternary: Reconstruction of material budget and current systems*, edited by Wefer,  
661 G., Mulitza, S. and Ratmeyer, V., Springer, Berlin, Heidelberg, New York, 21-46, 2003.
- 662
- 663 Fischer, G., Karakas, G., Blaas, M., Ratmeyer, V., Nowald, N., Schlitzer, R., Helmke, P., Davenport, R.,  
664 Donner, B., Neuer, S., and Wefer, G.: Mineral ballast and particle settling rates in the coastal upwelling  
665 system off NW Africa and the South Atlantic. 98, 281–298, doi:10.1007/s00531-007-0234-7, 2009a.
- 666 Fischer, G., Reuter, C., Karakas, G., Nowald, N., and Wefer, G.: Offshore advection of particles within the  
667 Cape Blanc filament, Mauritania: Results from observational and modelling studies. *Prog. Oceanogr.*, 83,  
668 322–330, 2009b.
- 669 Fischer, G., and Karakas, G.: Sinking rates and ballast composition of particles in the Atlantic Ocean:  
670 implications for the organic carbon fluxes to the deep ocean. *Biogeosciences* 6, 85–102, 2009.
- 671 Fischer, G., S. Neuer, R. Davenport, O. Romero, V. Ratmeyer, B. Donner, T. Freudenthal, H. Meggers and  
672 G. Wefer. The Northwest African Margin. In: *Carbon and Nutrient Fluxes in Continental Margins: A  
673 Global Synthesis*, edited by Liu, K. K., Atkinson, L., Quinones, R., Talaue-McManaus, L., IGBP Book  
674 Series, Springer, Berlin, 77-103. 2010.
- 675 Fontaine, B., Roucou, P., Gaetani, M., and Marteau, R.: Recent changes in precipitation, ITCZ convection  
676 and northern tropical circulation over North Africa (1979-2007). *Int. J. Climatol.*, 31, 633-648, 2011.
- 677 Fréon, P., Barange, M., and Aristegui, J.: Eastern Boundary Upwelling Ecosystems: integrative and  
678 comparative approaches. *Prog. Oceanogr.*, 83, 1–14, 2009.
- 679 Friese, C., van der Does, M., Merkel, U., Iversen, M., Fischer, G., and Stuut, J.-B.: Environmental factors  
680 controlling the seasonal variation in particle size of modern Saharan dust deposited offshore Cape, Blanc.  
681 *Aeolian Res.*, in press , 2016.
- 682 Goudie, A.S., and Middleton, N.J.: Saharan dust storms: nature and consequences. *Earth Sci. Rev.*, 56, 179-  
683 204, 2001.
- 684 Hedges, J.I., Baldock, J.A., Gelinias, Y., Lee, C., Peterson, M.L., and Wakeham, S.G.: The biochemical and  
685 elemental compositions of marine plankton: a NMR perspective. *Marine Chemistry* 78 (1), 47–63, 2002.

- 686 Helmke, P., Romero, O., and Fischer, G.: Northwest African upwelling and its effect on off-shore organic  
687 carbon export to the deep sea, *Global Biogeochem. Cy.*, 19, GB4015, doi:10.1029/2004GB002265, 2005.
- 688 Hsu, N.C., Gautam, R., Sayer, A.M., Bettenhausen, C., Li, C., Jeong, M.J., Tsay, S.-C., and Holben, B.N.:  
689 Global and regional trends of aerosol optical depth over land and ocean using SeaWiFS measurements  
690 from 1997-2010. *Atmos. Chem. Phys.*, 12, 8037-8053, 2012.
- 691 Hurrell, J.W.: NAO Index Data provided by the Climate Analysis Section, NCAR, Boulder, USA, Updated  
692 regularly. Accessed 01 January 2012, 1995.
- 693 Iversen, M.H., and Ploug, H.: Ballast minerals and the sinking carbon flux in the ocean: carbon-specific  
694 respiration rates and sinking velocities of marine snow aggregates. *Biogeosciences* 7, 2613–2624.  
695 <http://dx.doi.org/10.5194/bg-7-2613-2010>, 2010.
- 696 Iversen, M.H., Nowald, N., Ploug, H., Jackson, G.A., and Fischer, G.: High resolution profiles of vertical  
697 particulate organic matter export off Cape Blanc, Mauritania: degradation processes and ballasting  
698 effects. *Deep Sea Res. I*, 57, 771–784, 2010.
- 699 Iversen, M.H. and Robert, M.L.: Ballasting effects of smectite on aggregate formation and export from a  
700 natural plankton community. *Marine Chem.*, 175, 18-27, 2015.
- 701 Jickells, T.D., An, Z.S., Andersen, K.K., Baker, A.R., Bergametti, G., Brooks, N., Cao, J.J., Boyd, P.W.,  
702 Duce, R.A., Hunter, K.A., Kawahata, H., Kubilay, N., laRoche, J., Liss, P.S., Mahowald, N., Prospero,  
703 J.M., Ridgwell, A.J., Tegen, I., and Torres, R.: Global iron connections between desert dust, ocean  
704 biogeochemistry, and climate. *Science*, 308 (5718), 67–71, 2005.
- 705 Kahru, M., and Mitchell, B. G.: Ocean colour reveals increased blooms in various parts of the world ocean.  
706 *EOS* 89, 170, 2008.
- 707 Kalberer, M., G. Fischer, J. Pätzold, B. Donner, M. Segl and Wefer, G.: Seasonal sedimentation and stable  
708 isotope records of pteropods off Cape Blanc. *Marine Geol.*, 113, 305-320, 1993.
- 709 Karakas, G., Nowald, N., Blaas, M., Marchesiello, P., Frickenhaus, S., and Schlitzer, R.: High-resolution  
710 modeling of sediment erosion and particle transport across the northwest African shelf. *J. Geophys. Res.*,  
711 111. C06025, <http://dx.doi.org/10.1029/2005JC003296>, 2006.
- 712 Karakas, G., Nowald, N., Schäfer-Neth, C., Iversen, M.H., Barkmann, W., Fischer, G., Marchesiello, P., and  
713 Schlitzer, R.: Impact of particle aggregation on vertical fluxes of organic matter. *Prog. Oceanogr.* 83,  
714 331–341, 2009.
- 715 Kaufman, Y. J., Koren, I., Remer, L. A., Tanré, D., Ginoux, P., and Fan, S.: Dust transport and deposition  
716 from the Terra-Moderate Resolution Imaging Spectroradiometer (MODIS) spacecraft over the Atlantic  
717 Ocean, *J. Geophys. Res.*, 110, D10S12, doi:10.1029/2003JD004436, 2005.
- 718 Klaas, C., and Archer, D.E.: Association of sinking organic matter with various types of ballast in the deep  
719 sea: Implications for the rain ratio, *Global Biogeochem. Cycles*, 16(4), 1116,  
720 doi:10.1029/2001GB001765, 2002.
- 721 Kremling, K., Lentz, U., Zeitzschell, B., Schulz-Bull, D.E., and Duinker, J.C.: New type of time-series  
722 sediment trap for the reliable collection of inorganic and organic trace chemical substances. *Rev. Scient.*  
723 *Instr.*, 67, 4360–4363, 1996.
- 724 Kushnir, Y.: Interdecadal variations in North Atlantic sea surface temperature and associated  
725 atmospheric conditions. *J. of Climate*, 7(1), 141-157, 1994.
- 726 Lathuilière, C., Echevin, V., and Levy, M.: Seasonal and intraseasonal surface chlorophyll-a variability along  
727 the northwest African coast. *J. Geophys. Res., Oceans*, 13 (C5), C05007, doi:10.1029/2007/JC004433,  
728 2008.
- 729 Lucio, P.S., Baldicero Molion, L.C., de Avial-Valadao, C.E., Conde, F.C., Malheiro Ramos, A., and Dias de  
730 Melo, M.L.: Dynamical outlines of the rainfall variability and the ITCZ role over the West Sahel.,  
731 *Atmospheric Climate Sci.*, 2, 337-350, 2012.
- 732 Marcello, J., Hernandez-Guerra, A., Eugenio, F., and Fonte, A.: Seasonal and temporal study of the  
733 northwest African upwelling system. *Internat. J. Remote Sens.*, 32, 7, 1843-1859, 2011.

- 734 McGregor, H.V., Dima, M., Fischer, H.W., and Multiza, S.: Rapid 20<sup>th</sup> century increase in coastal upwelling  
735 off Northwest Africa. *Science*, 315, 637-639, 2007.
- 736 Meunier, T., Barton, E.D., Barreiro, B., and Torres, R.: Upwelling filaments off Cape Blanc: interaction of  
737 the NW African upwelling current and the Cape Verde frontal zone eddy field? *J. Geophys. Res., Oceans*,  
738 117 (C8), C08031, doi:10.1029/2012JC007905, 2012.
- 739 Mittelstaedt, E.: The ocean boundary along the northwest African coast: Circulation and oceanographic  
740 properties at the sea surface: *Prog. Oceanogr.*, 26, 307–355, 1991.
- 741 Moulin, C. and Chiapello, I.: Evidence of the control of summer atmospheric transport of African dust over  
742 the Atlantic by Sahel sources from TOMS satellites (1979-2000). *Geophys. Res. Lett.*, 31, L02107,  
743 doi:10.1029/2003GL019031, 2004.
- 744 Müller P.J. and Schneider, R.: An automated leaching method for the determination of opal in sediments and  
745 particulate matter. *Deep Sea Res. I*, 40, 425-444, 1993.
- 746 Muller-Karger, F. E., Varela, R., Thunell, R., Luerssen, R., Hu, C., and Walsh, J. J.: The importance of  
747 continental margins in the global carbon cycle, *Geophys. Res. Lett.*, 32, L01602,  
748 doi:10.1029/2004GL021346, 2005.
- 749 Narajan, N., Paul, A., and Schulz, M.: Trends in coastal upwelling intensity during the late 20th century.  
750 *Ocean Sci.*, 6, 815-823, 2014.
- 751 Neuer, S., Torres-Padron, M.E., Gelado-Caballeo, M.D., Rueda, M.J., Hernandez-Brito, J., Davenport, R.,  
752 and Wefer, G.: Dust deposition to the eastern subtropical North Atlantic gyre: Does ocean's  
753 biogeochemistry respond? *Global Biogeochem. Cy.*, 18, GB4020,  
754 <http://dx.doi.org/10.1029/2004GB002228>, 2004.
- 755 Nicholson, S.E.: The West African Sahel: A review of recent studies on the rainfall regime and its  
756 interannual variability. *ISRN Meteorology*, 2013, 453521, doi:10.1155/2013/453521, 2013.
- 757 Nowald, N., Iversen, M.H., Fischer, G., Ratmeyer, V., and Wefer, G.: Time series of in-situ particle  
758 properties and sediment trap fluxes in the coastal upwelling filament off Cape Blanc, Mauritania. *Prog.*  
759 *Oceanogr.*, 137, Part A, 1–11, 2015, doi:10.1016/j.pocean.2014.12.015, 2015.
- 760 N'Tchayi Mbourou, G., Berrand, J.J., and Nicholson, S.E.: The diurnal and seasonal cycles of wind-borne  
761 dust over Africa north of the equator. *J. Appl. Meteorology*, 36, 868-882, 1997.
- 762 Nykjaer, L., and Van Camp, L.: Seasonal and interannual variability of coastal upwelling along northwest  
763 Africa and Portugal from, 1981 to 1991. *J. Geophys. Res.*, 99, 197–207, 1994.
- 764 Pauly, D., and Christensen, V.: Primary production required to sustain global fisheries. *Nature*, 374, 255-257,  
765 1995.
- 766 Ploug, H., Iversen, M.H., and Fischer, G.: Ballast, sinking velocity, and apparent diffusivity within marine  
767 snow and zooplankton fecal pellets: implications for substrate turnover by attached bacteria. *Limnol.*  
768 *Oceanogr.*, 53 (5), 1878–1886, 2008.
- 769 Pradhan, Y., Lavender, S.J., Hardman-Mountford, N.J., and Aiken, J.: Seasonal and inter-annual variability  
770 of chlorophyll-a concentration in the Mauritanian upwelling: observation of an anomalous event during  
771 1998–1999. *Deep Sea Res. II*, 53, 1548–1559, 2006.
- 772 Prospero, J.M.: Mineral-aerosol transport to the North Atlantic and North Pacific: The impact of African and  
773 Asian sources. In: *The long range atmospheric transport of natural and contaminant substances*, edited by  
774 Knap, A.H., Dordrecht, Mathematical and Physical Sciences. Kluwer Academic Publishers, 19–52, 1990.
- 775 Prospero, J.M., and Lamb, P.J.: African droughts and dust transport to the Caribbean: climate change  
776 implications. *Science*, 302, 1024-1027, 2003.
- 777 Ratmeyer, V., Fischer, G. and Wefer, G.: Lithogenic particle fluxes and grain size distributions in the deep  
778 ocean off northwest Africa: Implications for seasonal changes of aeolian dust input and downward  
779 transport, *Deep-Sea Res. II*, 46, 1289-1337, 1999a.
- 780 Ratmeyer, V., Balzer, W., Bergametti, G., Chiapello, I., Fischer, G., and Wyputta, U.: Seasonal impact of  
781 mineral dust on deep-ocean particle flux in the eastern subtropical Atlantic Ocean, *Mar. Geol.*, 159, 241–  
782 252, 1999b.

- 783 Redfield, A. C., Ketchum, B.H., and Richards, F.A.: The influence of organisms on the composition of  
784 seawater. In: The Sea, edited by Hill, M.N., Vol. 2, Wiley and Sons, Chichester, 26-77, 1963.
- 785 Romero, O.E., Lange, C.B., Swap, R.J., and Wefer, G.: Eolian-transported freshwater diatoms and phytoliths  
786 across the equatorial Atlantic record temporal changes in Saharan dust transport patterns. *J. Geophys.*  
787 *Res.*, 104, 3211-3222, 1999.
- 788 Romero, O.E., Lange, C.B., and Wefer, G.: Interannual variability (1988-1991) of siliceous phytoplankton  
789 fluxes off northwest Africa. *J. Plank. Res.*, 24 (10), 1035-1046, doi:10.1093/plankt/1024.1010.1035,  
790 2002.
- 791 Romero, O. E., Kim, J.-H. , and Donner, B.: Submillennial-to-millennial variability of diatom production off  
792 Mauritania, NW Africa, during the last glacial cycle, *Paleoceanography*, 23, PA3218,  
793 doi:10.1029/2008PA001601, 2008.
- 794 Shanahan, T. M., Overpeck, J. T., and Anchukaitis, K. J., Beck, J. W., Cole, J. E., Dettman, D. L., Peck, J.  
795 A., Scholz, C. A., and King, J. W.: Atlantic Forcing of persistent drought in West Africa, *Science*, 324,  
796 377–380, 2009.
- 797 Siegel, D.A., and Deuser, W.G.: Trajectories of sinking particles in the Sargasso Sea: modeling of statistical  
798 funnels above deep-ocean sediment traps. *Deep-Sea Res. I*, 44 (9–10), 1519–1541, 1997.
- 799 Ternon, E., Guieu, C., Loye-Pilot, M.-D., Leblond, N., Bosc, E., Gasser, B., Miquel, J.C., and Martin, J.: The  
800 impact of Saharan dust on the particulate export in the water column of the North Western Mediterranean  
801 Sea. *Biogeosciences* 7, 809–826, 2010.
- 802 Thunell, R., Benitez-Nelson, C., Varela, R., Astor, Y., and Muller-Karger, F.: Particulate organic carbon  
803 fluxes along upwelling-dominated continental margins: rates and mechanisms. *Glob. Biogeochem. Cy.*,  
804 21, GB1022, doi:10.1029/2006GB002793, 2007.
- 805 Van Camp, L., Nykjær, L., Mittelstaedt, E., and Schlittenhardt, P.: Upwelling and boundary circulation off  
806 Northwest Africa as depicted by infrared and visible satellite observations. *Prog. Oceanogr.*, 26, 357–402,  
807 1991.
- 808 Yeager, S. G., Shields, C.A., Large, W.G., and Hack, J.J. : The Low-Resolution CCSM3, *J. Climate*, 19,  
809 2545-2566, 2006.
- 810 Yu E. F., Francois R., Honjo S., Flerer A.P., Manganini S.J., Rutgers van der Loeff, M.M., and Ittekkot V.:  
811 Trapping efficiency of bottom-tethered sediment traps estimated from the intercepted fluxes of <sup>230</sup>Th and  
812 <sup>231</sup>Pa. *Deep-Sea Res. I*, 48, 865-889, 2001.
- 813 Zeeberg, J., Corten, A., Tjoe-Awie, P., Coca, J., and Hamady, B.: Climate modulates the effects of  
814 *Sardinella aurita* fisheries off Northwest Africa, *Fish. Res.*, 89, 65–75, 2008.
- 815 Zenk, W., Klein, B., and Schroder, M.: Cape Verde Frontal Zone. *Deep Sea Res. I*, 38, 505–530, 1991.
- 816 Zhao, T. X.-P., Laszlo, I., Guo, W., Heidinger, A., Cao, C., Jelenak, A., Tarpley, D., and Sullivan, J.: Study  
817 of long-term trend in aerosol optical thickness observed from operational AVHRR satellite instrument, *J.*  
818 *Geophys. Res.*, 113, D07201, doi:10.1029/2007JD009061, 2008.
- 819

820 **Figure Captions**

821 Fig. 1. General setting of the study area: a: Oceanographic setting in the area of the long-term mooring site  
 822 Cape Blanc ( $CB_{meso}$ ) within the Cape Blanc filament (green arrow), dissolving into eddies (indicated as  
 823 circles with arrows) further offshore. The Cape Verde Frontal Zone (CVFZ) separating the subsurface water  
 824 masses of the NACW and the SACW (Zenk et al., 1991) is shown. Upwelling zones are marked according to  
 825 Cropper et al. (2014). Ocean colour map (chlorophyll, 9 km resolution) from MODIS is shown for two  
 826 extreme years, winter 2006-2007 (b: NAO+) and winter 2009-2010 (c: NAO-). SeaWiFS ocean colour  
 827 during two contrasting situations for the strongest ENSO cycle 1997-1999: fall 1997 during the warm El  
 828 Niño phase (d), and fall 1998 during the cold La Niña event (e). The study site  $CB_{meso}$  is indicated by a  
 829 square box in the ocean colour pictures, green arrow indicates the Cape Blanc filament, yellow arrows the  
 830 major dust transport. *MC=Mauritanian Current, CC=Canary Current, NEC=North Equatorial Current.*

831  
 832 Fig. 2. The NAO Hurrell index (DJFM, station-based, Lisbon-Rejkjavik, Hurrell, 1995) plotted from 1864 to  
 833 2014. Grey shading indicates the time period covered by the long-term flux record off Cape Blanc,  
 834 Mauritania. A 5-point running mean is shown by the thick line.

835  
 836 Fig. 3: Teleconnections affecting the study site off Cape Blanc. Correlation of simulated sea-level pressure  
 837 (SLP) with a: the NAO SLP index after Hurrell (Hurrell, 1995; boreal winter season), b: the Nino3 SST  
 838 index (boreal winter season), and c: North Atlantic SST (low pass-filter applied considering periods above  
 839 10 years). Analysis based on the last 100 model years of a present-day control simulation using the CCSM3  
 840 model.

841  
 842 Fig. 4. Seasonal means of major bulk fluxes of the lower traps only (a: total, b: organic carbon, c: nitrogen,  
 843 d: biogenic silica (=BSi), e: carbonate, and f: lithogenic=mineral dust) and the respective standard deviations  
 844 (1 s.d.), which reflect interannual variability. Relative contributions (%) of BSi, organic carbon, nitrogen,  
 845 carbonate and lithogenic materials to total mass in the respective seasons are indicated by numbers below the  
 846 bars.

847  
 848 Fig. 5. a: Total mass fluxes of the lower traps (grey-shaded). Gaps were filled with upper trap data (light grey  
 849 bars). Deviations of the seasonal total mass fluxes from the long-term seasonal means (anomalies), fitted  
 850 with a 9-order polynomial (b). c: Atlantic Multidecadal Oscillation (AMO) Index based on monthly SST  
 851 fitted with a 9th-order polynomial fit (dashed blue line). The strong ENSO cycle 1997-1999 with a warm El  
 852 Niño and a cold La Niña phase is indicated.

853  
 854 Fig. 6. a: Seasonal flux of biogenic silica (BSi, green) with gaps filled from the upper trap data (light green  
 855 bars). Deviations of the long-term seasonal means (anomalies, b). c: The NAO Hurrell index (DJFM). d:  
 856 Seasonal chlorophyll concentration both from the MODIS (light green) and the SeaWiFS (dark green)  
 857 sensors at 9 km resolution. Note that high chlorophyll biomass is generally occurring in spring but

858 sometimes in summer/fall as well (e.g. in 1998, 2007). SeaWiFS chlorophyll reveals a decreasing trend from  
859 1997 to 2010, not mimicked in any flux data. The strong ENSO cycle 1997-1999 with a warm El Niño and a  
860 cold La Niña phase is indicated.

861

862 Fig. 7. a: The NAO Hurrell index (DJFM, Hurrell, 1995) plotted against winter BSi fluxes from Fig. 6. Note  
863 the increase of BSi with increasing NAO index. However, the relationship is weak due to unusual  
864 sedimentation events in the years 1998-99, 2002, 2004, and, in particular in 2005. When omitting the data  
865 point from 2005, the correlation coefficient increases, but remains low ( $R^2=0.14$ ,  $N=20$ ). Upper trap flux data  
866 from winter 1998 and 2004 may be too low as the filament with elevated chlorophyll was small and the  
867 particles did not reach the upper trap (see text). Omitting these two data point would slightly improve the  
868 relationship.

869 b: The size of the Cape Blanc filament (Fischer et al., 2009) during winter months (DJFM) versus winter  
870 BSi fluxes shows higher fluxes with larger filament size. When omitting the BSi flux from winter 2005, a  
871 statistically significant relationship between filament size and fluxes is obtained ( $R^2=0.63$ ,  $N=10$ ). Years  
872 given in the figure denote the respective winter seasons (e.g. 1999 = Dec 1998 – Mar 1999).

873

874 Fig. 8. a: Seasonal flux of lithogenic (=mineral dust) particles (orange) with gaps filled from the upper trap  
875 data (light orange bars). Deviations from the long-term seasonal means (anomalies, b). Note the large  
876 positive anomalies with longer duration in 1988-89, 1997-2000 and 2005-2006. From about 2000 to 2004-  
877 2005, lithogenic fluxes remain rather low. In 2005, dust sedimentation and BSi flux (Fig. 6b) were high  
878 throughout the year. c: The AOT from the SeaWiFS (brown) and MODIS (light brown) sensors shows  
879 repeatedly high values in summer, but not in winter when dust sedimentation is highest in the study area. A  
880 typical short-term (2-day) dust storm in January 2012 is shown as insert in the upper right. The strong  
881 ENSO cycle 1997-1999 with a warm El Niño and a cold La Niña phase is indicated.

882

883 Fig. 9. Relationships between BSi and lithogenic (= mineral dust) fluxes for the winter (a) and summer (b)  
884 seasons. Note the high correspondence in winter ( $R^2=0.78$ ,  $N=21$ ); a lower coefficient is found for the  
885 summer season. During the outstanding year of 2005 (see Fig. 7), both points for winter and summer are  
886 close to the linear regression line.

887

888 Fig. 10. a: Seasonal flux of total carbonate (blue) with gaps filled from the upper trap data (light blue bars).  
889 Deviations from the long-term seasonal means (anomalies, b). c: Seasonal flux of pteropods. During the  
890 strongest ENSO cycle 1997-2000, longer periods of low and high carbonate fluxes occurred. Note the  
891 episodic sedimentation pattern of pteropods with maxima e.g. in summer 1998, 2002 and 2004. The strong  
892 ENSO cycle 1997-1999 with a warm El Niño and a cold La Niña phase is indicated.

893

894



895 Table 1. Deployment data of the moorings and traps at the mesotrophic sediment trap site CB, Cape Blanc,  
896 Mauritania. Associated ships' cruises and references to earlier publications on fluxes are indicated.

Trap name	LAT N	LONG W	water depth m	trap depth m	sampling start	end	no of samples	remark, reference to fluxes	relevant cruise recovery/ GeoB no.
CB-1 lower	20°45.3'	19°44.5'	3646	2195	22.03.88	08.03.89	13	<i>Fischer et al. 1996, 2003</i>	Meteor 9/4/ GeoB 1121-4
CB-2 lower	21°08.7'	20°41.2'	4092	3502	15.03.89	24.03.90	22	<i>Fischer et al. 1996, 2003</i>	Meteor 12/1/ GeoB 1230-1
CB-3 lower	21°08.3'	20°40.3'	4094	3557	29.04.90	08.04.91	17	<i>Fischer et al. 1996, 2003, 2010</i>	Polarstern ANT IX/4
CB-4 lower	21°08.7'	20°41.2'	4108	3562	03.03.91	19.11.91	13	<i>Fischer et al. 1996, 2003, 2010</i>	Meteor 20/1/ GeoB 1602-1
CB-5 lower	21°08.6'	20°40.9'	4119	3587	06.06.94	27.08.94	19		Meteor 29/3/ GeoB 2912-1
CB-6 upper	21°15.0'	20°41.8'	4137	771	02.09.94	25.10.95	20	<i>Fischer et al. 2010</i>	Polarstern ANT XIII/1
CB-7 lower	21°15.4'	20°41.8'	4152	3586	20.11.95	29.01.97	20		Meteor 38/1/ GeoB 4302-7
CB-8 upper	21°16.3'	20°41.5'	4120	745	30.01.97	04.06.98	20	<i>Fischer et al. 2010</i>	Meteor 41/4/ GeoB 5210-2
CB-9 lower	21°15.2'	20°42.4'	4121	3580	11.06.98	07.11.99	20	<i>Helmke et al. 2005</i>	Meteor 46/1/ GeoB 6103-3
CB-10 lower	21°17.2'	20°44.1'	4125	3586	10-10- 10.11.99	00	3	mostly no seasonal sampling	Polarstern ANT XVIII/1
CB-11 upper	21°16.8'	20°43.0'	4113	1003	11.10.00	30.03.01	20		Poseidon 272/ GeoB 7401-1
CB-12 lower	21°16.0'	20°46.5'	4145	3610	05.04.01	22.04.02	14		Meteor 53/1c/ GeoB 7917-1
CB-13 lower	21°16.8'	20°46.7'	4131	3606	23.04.02	08.05.03	20	<i>Fischer et al., 2009</i> <i>Fischer and Karkas, 2009</i>	Meteor 58/2b/ GeoB 8628-1
CB-14 upper	21°17.2'	20°47.6'	4162	1246	31.05.03	05.04.04	20		Poseidon 310/ no number
CB-15 lower	21°17.9'	20°47.8'	4162	3624	17.04.04	21.07.05	20		Meteor 65/2/ no number
CB-16 lower	21°16.8'	20°47.8'	4160	3633	25.07.05	28.09.06	20		Poseidon 344/1/ GeoB 11401-1
CB-17 lower	21°16.4'	20°48.2'	4152	3614	24.10.06	25.03.07	20		Merian 04/b/ GeoB 11833-1
CB-18 lower	21°16.9'	20°48.1'	4168	3629	25.03.07	05.04.08	20		Poseidon 365/2/ GeoB 12907-1
CB-19 lower	21°16.2'	20°48.7'	4155	3617	22.04.08	22.03.09	20		Merian 11/2/ GeoB 13616-4
CB-20 upper	21°15.6'	20°50.7'	4170	1224	03.04.09	26.02.10	19		Poseidon 396/ GeoB 14201-3
CB-21 lower	21°15.6'	20°50.9'	4155	3617	28.02.10	04.04.11	20		Merian 18/1/ GeoB 15709-1
CB-22 lower	21°16.1'	20°50.9'	4160	3622	05.05.11	11.01.12	15		Poseidon 425/ GeoB 16101-1
CB-23 lower	21°15.8'	20°52.4'	4160	3622	20.01.12	22.01.13	18		Poseidon 445/ GeoB 17102-5

898 Table 2. Seasonal flux data and percentages of major bulk components of total flux at the mesotrophic sediment trap site CB from 1988 to 2012.

CB meso	interval		sample no. of trap	season	year	duration days	remark	TTL mass	BSi	org. carbon	nitrogen	carbonate	lithogenic	BSi	org. carbon	nitrogen	carb.	lith.
	start	end						g m <sup>-2</sup>	g m <sup>-2</sup>	g m <sup>-2</sup>	g m <sup>-2</sup>	g m <sup>-2</sup>	g m <sup>-2</sup>	%	%	%	%	%
<b>CB-1 lower</b>	22.03.88	11.06.88	#1-3	spring	1988	81		15,64	1,91	0,59	0,069	4,89	7,66	12,23	3,77	0,44	31,25	48,96
	11.06.88	27.09.88	#4-7	summer		108		23,01	1,57	1,07	0,135	10,83	8,47	6,81	4,66	0,59	47,07	36,81
	27.09.88	17.12.88	#8-10	fall		81		14,12	0,86	0,51	0,056	6,78	5,46	6,11	3,60	0,40	48,00	38,70
	17.12.88	08.03.89	#11-13	winter	1989	81		11,50	0,89	0,45	0,055	5,09	4,63	7,70	3,92	0,48	44,21	40,23
<b>CB-2 lower</b>	15.03.89	25.06.89	#1-6	spring	1990	102		12,91	0,52	0,40	0,051	6,92	4,68	4,03	3,10	0,40	53,60	36,25
	25.06.89	18.09.89	#7-11	summer		85		13,62	0,49	0,39	0,046	7,48	4,87	3,60	2,86	0,34	54,92	35,76
	18.09.89	29.12.89	#12-17	fall		102		16,29	0,67	0,48	0,056	8,21	6,45	4,11	2,95	0,34	50,40	39,59
	29.12.89	24.03.90	#18-22	winter		85		14,06	0,75	0,46	0,055	6,81	5,58	5,33	3,27	0,39	48,44	39,69
<b>CB-3 lower</b>	29.04.90	03.07.90	#2-4	spring	1991	64,5		12,68	0,49	0,39	0,047	6,78	4,64	3,87	3,04	0,37	53,49	36,55
	03.07.90	27.09.90	#5-8	summer		86		13,20	0,40	0,39	0,044	7,35	4,67	3,05	2,98	0,33	55,64	35,35
	27.09.90	22.12.90	#9-12	fall		86		9,76	0,40	0,44	0,052	4,02	4,46	4,08	4,52	0,53	41,21	45,66
	22.12.90	18.03.91	#13-16	winter		86		10,89	0,58	0,73	0,091	4,50	4,34	5,33	6,73	0,84	41,35	39,87
<b>CB-4 lower</b>	18.03.91	22.06.91	#17 + #1-5	spring	1991	71,5	gap	4,87	0,24	0,38	0,053	2,09	1,77	4,89	7,83	1,09	43,02	36,36
	22.06.91	20.09.91	# 6-14	summer		90		9,06	0,48	0,83	0,110	3,66	3,25	5,30	9,16	1,21	40,40	35,87
	20.09.91	19.11.91	# 15-20	fall		60		2,67	0,13	0,17	0,023	1,31	0,89	4,87	6,37	0,86	49,06	33,33
no sampling																		
<b>CB-5 lower</b>	06.06.94	23.06.94	#1-4	spring	1994	17		1,76	0,05	0,05	0,007	1,27	0,35	2,84	2,84	0,40	72,16	19,89
	23.06.94	27.08.94	#5-19	summer		65		7,30	0,16	0,14	0,023	5,97	0,89	2,19	1,92	0,32	81,78	12,19
<b>CB-6 upper</b>	24.09.94	21.12.94	# 2-5	fall	1995	88		11,58	0,26	0,70	0,104	6,82	3,10	2,27	6,02	0,90	58,92	26,74
	21.12.94	19.03.95	# 6-9	winter		88		12,44	0,96	0,74	0,113	5,89	4,12	7,69	5,91	0,91	47,33	33,14
	19.03.95	15.06.95	# 10-13	spring		88		3,50	0,22	0,24	0,042	1,59	1,20	6,29	6,86	1,20	45,43	34,29
	15.06.95	11.09.95	# 14-17	summer		88		0,24	0,00	0,00	0,001	0,00	0,00	0,00	0,00	0,42	0,00	0,00
<b>CB-7 lower</b>	20.11.95	19.12.95	#1	fall	1996	29		2,91	0,18	0,12	0,015	1,22	1,26	6,26	4,26	0,52	42,06	43,33
	19.12.95	16.03.96	#2-5	winter		88		8,02	0,37	0,34	0,044	3,80	3,16	4,55	4,28	0,55	47,40	39,48
	16.03.96	12.06.96	#6-9	spring		88		9,55	0,63	0,61	0,080	4,76	2,94	6,58	6,38	0,84	49,83	30,82
	12.06.96	30.09.96	#10-14	summer		110		7,44	0,20	0,29	0,036	4,72	1,95	2,66	3,90	0,48	63,39	26,15
	30.09.96	27.12.96	#15-18	fall		88		8,59	0,38	0,40	0,049	3,73	3,69	4,40	4,64	0,57	43,38	42,91

Table 2. continued

CB meso	interval		sample no. of trap	season	year	duration days	remark	TTL mass	BSi	org. carbon	nitrogen	carbonate	lithogenic	BSi	org. carbon	nitrogen	carb.	lith.
	start	end						g m <sup>-2</sup>	g m <sup>-2</sup>	g m <sup>-2</sup>	g m <sup>-2</sup>	g m <sup>-2</sup>	%	%	%	%	%	
<b>CB-7/8 lower</b>	27.12.96	20.03.97	#19-20 + #1-2	winter	1997	82		14,24	0,78	0,77	0,097	5,37	6,55	5,46	5,41	0,68	37,70	46,00
<b>CB-8 upper</b>	20.03.97	20.06.97	# 3-6	spring		98		17,72	0,62	1,05	0,131	9,69	5,30	3,50	5,94	0,74	54,68	29,92
	20.06.97	02.10.97	# 7-10	summer		98		4,25	0,04	0,20	0,026	2,91	0,90	0,92	4,66	0,61	68,50	21,20
	02.10.97	14.12.97	# 11-13	fall		73,5		0,49	0,01	0,04	0,006	0,25	0,12	2,86	7,14	1,22	51,84	24,08
	14.12.97	22.03.98	# 14-17	winter	1998	98		1,68	0,05	0,15	0,024	0,84	0,45	3,21	8,87	1,43	50,12	26,49
	22.03.98	18.06.98	#18-20 + #1	spring		81	gap	1,57	0,01	0,06	0,008	1,21	0,20	0,45	3,70	0,51	76,80	12,62
<b>CB-9 lower</b>	18.06.98	09.09.98	# 2-4	summer		82,5		17,67	0,61	0,58	0,074	12,57	3,34	3,45	3,29	0,42	71,11	18,87
	09.09.98	28.12.98	# 5-8	fall		110		17,06	1,07	0,77	0,086	9,31	5,15	6,25	4,48	0,50	54,59	30,19
	28.12.98	20.03.99	# 9-11	winter	1999	82,5		16,33	1,19	0,62	0,073	7,18	6,71	7,27	3,81	0,45	43,99	41,11
	20.03.99	11.06.99	# 12-14	spring		82,5		19,55	1,08	0,65	0,083	11,77	5,40	5,53	3,33	0,42	60,17	27,61
	11.06.99	29.09.99	# 15-18	summer		110		16,88	0,51	0,57	0,068	11,80	3,43	3,02	3,35	0,40	69,92	20,35
<b>CB-9/10 lower</b>	29.09.99	16.12.99	#19-20+ #1-2	fall		75	gap	2,20	0,09	0,09	0,010	1,11	0,75	4,26	3,90	0,45	50,36	34,07
	16.12.99	21.03.00	#3	winter	2000	94		8,92	0,14	0,45	0,076	7,26	0,93	1,59	5,04	0,85	81,39	10,46
	21.03.00	21.06.00	#3	spring		92		8,74	0,14	0,44	0,075	7,11	0,91	1,59	5,05	0,86	81,33	10,45
	21.06.00	21.09.00	#3	summer		92		8,74	0,14	0,44	0,075	7,11	0,91	1,59	5,05	0,86	81,33	10,45
<b>CB-11 upper</b>	11.10.00	18.12.00	#3 + # 1-8	fall		87		8,32	0,41	0,56	0,087	5,13	1,68	4,93	6,73	1,05	61,66	20,19
	18.12.00	22.03.01	#9-19	winter	2001	93,5		6,51	0,39	0,60	0,093	3,57	1,34	6,01	9,25	1,43	54,84	20,58
<b>CB-12 lower</b>	05.04.01	27.06.01	# 1-4	spring		83		6,50	0,32	0,25	0,034	2,91	2,76	4,92	3,85	0,52	44,77	42,46
	27.06.01	01.10.01	# 5-9	summer		96,25		12,49	1,03	0,63	0,091	6,47	3,75	8,25	5,04	0,73	51,80	30,02
	01.10.01	17.12.01	# 10-13	fall		77		7,90	0,53	0,43	0,050	3,72	2,79	6,71	5,44	0,63	47,09	35,32
	17.12.01	21.03.02	# 14 sammel	winter	2002	94,25		0,88	0,05	0,04	0,009	0,75	0,02	5,68	4,20	1,02	85,23	2,27
<b>CB-13 lower</b>	23.04.02	19.06.02	#1-3	spring		57		6,03	0,27	0,23	0,029	3,53	1,78	4,46	3,78	0,48	58,42	29,55
	19.06.02	22.09.02	#4-8	summer		95		23,10	1,03	0,62	0,085	16,85	3,98	4,44	2,69	0,37	72,94	17,23
	22.09.02	26.12.02	#9-13	fall		95		9,51	0,42	0,32	0,042	5,53	2,92	4,42	3,36	0,44	58,16	30,66
	26.12.02	31.03.03	#14-18	winter	2003	95		11,41	0,55	0,35	0,050	6,78	3,39	4,78	3,07	0,44	59,37	29,72
	31.03.03	08.05.03	#19-20	spring		38		7,71	0,69	0,27	0,036	3,68	2,79	8,92	3,54	0,47	47,73	36,23

Table 2. continued

CB meso	interval		sample no. of trap	season	year	duration days	remark	TTL mass	BSi	org. carbon	nitrogen	carbonate	lithogenic	BSi	org. carbon	nitrogen	carb.	lith.
	start	end						g m <sup>-2</sup>	g m <sup>-2</sup>	g m <sup>-2</sup>	g m <sup>-2</sup>	g m <sup>-2</sup>	%	%	%	%	%	
<b>CB-14 upper</b>	15.06.03	16.09.03	#2-7	summer		93		11,35	1,26	0,83	0,104	5,77	2,67	11,06	7,32	0,92	50,80	23,52
	16.09.03	18.12.03	#8-13	fall		93		8,28	0,84	0,45	0,061	3,99	2,56	10,16	5,48	0,74	48,14	30,87
	18.12.03	20.03.04	#14-19	winter	2004	93		0,58	0,03	0,03	0,005	0,29	0,16	5,39	5,22	0,87	49,91	27,48
<b>CB-15 lower</b>	17.04.04	25.06.04	#1-3	spring		69		12,49	0,66	0,45	0,059	7,58	3,36	5,30	3,58	0,47	60,64	26,90
	25.06.04	25.09.04	#4-7	summer		92		15,21	0,43	0,39	0,053	10,75	3,25	2,80	2,54	0,35	70,64	21,34
	25.09.04	26.12.04	#8-11	fall		92		8,34	0,48	0,36	0,043	4,22	2,93	5,72	4,25	0,52	50,60	35,14
	26.12.04	28.03.05	#12-15	winter	2005	92		23,56	1,69	1,12	0,152	12,18	7,44	7,18	4,76	0,65	51,69	31,59
<b>CB-16 lower</b>	28.03.05	28.06.05	#16-19	spring		92		7,72	0,24	0,28	0,041	5,00	1,93	3,04	3,65	0,53	64,72	24,94
	28.06.05	27.09.05	#20 + 1-3	summer		87,5	gap	18,23	1,12	0,63	0,078	10,46	5,40	6,13	3,43	0,43	57,38	29,62
	27.09.05	22.12.05	#4-7	fall		86		15,87	1,19	0,63	0,074	6,98	6,45	7,51	3,94	0,47	43,97	40,63
	22.12.05	18.03.06	#8-11	winter	2006	86		14,90	0,72	0,46	0,056	8,71	4,54	4,82	3,11	0,38	58,46	30,48
	18.03.06	12.06.06	#12-15	spring		86		15,16	0,92	0,66	0,085	9,04	3,87	6,09	4,37	0,56	59,64	25,51
<b>CB-17 lower</b>	12.06.06	28.09.06	#16-20	summer		107,5		6,07	0,45	0,24	0,031	3,55	1,58	7,38	3,97	0,51	58,51	26,11
	24.10.06	23.12.06	#1-8	fall		60		4,34	0,14	0,14	0,021	2,81	1,09	3,28	3,30	0,48	64,87	25,24
	23.12.06	23.03.07	#9-20	winter	2007	90		19,89	1,00	0,84	0,112	12,42	4,78	5,03	4,23	0,56	62,47	24,03
<b>CB-18 lower</b>	25.03.07	25.06.07	#1-5	spring		92		11,22	0,38	0,48	0,061	7,05	2,83	3,40	4,24	0,54	62,87	25,24
	25.06.07	28.09.07	#6-10	summer		95		8,57	0,29	0,33	0,040	4,79	2,83	3,43	3,83	0,47	55,94	32,96
	28.09.07	13.12.07	#11-14	fall		76		7,19	0,39	0,28	0,033	4,05	2,20	5,38	3,87	0,46	56,31	30,56
	13.12.07	17.03.08	#15-19	winter	2008	95		10,58	0,64	0,50	0,061	5,43	3,51	6,03	4,69	0,58	51,37	33,22
<b>CB-19 lower</b>	17.03.08	23.06.08	#20 + 1-4	spring		81	gap	5,49	0,24	0,22	0,029	4,04	0,76	4,43	4,03	0,53	73,67	13,92
	23.06.08	16.09.08	#5-9	summer		85		12,59	0,82	0,63	0,072	8,95	1,58	6,51	4,99	0,57	71,12	12,58
	16.09.08	27.12.08	#10-15	fall		102		9,01	0,47	0,44	0,045	4,64	3,03	5,17	4,87	0,50	51,45	33,60
	27.12.08	22.03.09	#16-20	winter	2009	85		9,51	0,63	0,42	0,050	6,56	1,47	6,60	4,44	0,53	69,04	15,47

905

Table 2.continued

CB meso	interval		sample no. of trap	season	year	duration days	remark	TTL mass	BSi	org. carbon	nitrogen	carbonate	lithogenic	BSi	org. carbon	nitrogen	carb.	lith.
	start	end						g m <sup>-2</sup>	g m <sup>-2</sup>	g m <sup>-2</sup>	g m <sup>-2</sup>	g m <sup>-2</sup>	%	%	%	%	%	
<b>CB-20 upper</b>	03.04.09	30.06.09	#1-5	spring		88		9,74	0,23	0,44	0,060	8,63	0,07	2,36	4,56	0,62	88,59	0,67
	30.06.09	28.09.09	#6-10	summer		90		3,25	0,09	0,16	0,021	2,63	0,21	2,74	4,95	0,65	80,90	6,43
	28.09.09	21.12.11	#11-(15)	fall		84		0,26	0,01	0,02	0,002	0,16	0,06	2,31	6,92	0,77	61,54	22,31
	21.12.11	26.02.10	#(11)- 19	winter	2010	67,5		18,77	0,66	0,95	0,086	10,78	5,42	3,54	5,07	0,46	57,45	28,85
<b>CB-21 lower</b>	20.03.10	28.06.10	#2-6	spring		100		7,34	0,24	0,31	0,047	4,78	1,33	3,27	4,26	0,64	65,12	18,12
	28.06.10	16.09.10	#7-10	summer		80		7,72	0,27	0,27	0,040	6,01	0,69	3,50	3,48	0,52	77,85	8,94
	16.09.10	25.12.10	#11-15	fall		100		9,81	0,26	0,50	0,041	6,00	2,55	2,65	5,13	0,42	61,16	25,99
	25.12.10	15.03.11	#16-19	winter	2011	80		4,94	0,20	0,20	0,029	3,44	0,89	4,05	4,13	0,59	69,64	18,02
<b>CB-21/22 lower</b>	15.03.11	21.06.11	#20 + 1-3	spring		67	gap	4,90	0,18	0,21	0,028	3,93	0,46	3,61	4,23	0,57	80,22	9,39
	21.06.11	14.09.11	#4-8	summer		85		10,45	0,28	0,54	0,048	7,86	1,23	2,63	5,16	0,46	75,22	11,77
	14.09.11	25.12.11	#9-14	fall		102		12,52	0,46	0,56	0,057	8,92	2,02	3,65	4,43	0,46	71,25	16,13
<b>CB-22/23 lower</b>	25.12.11	24.03.12	#15 +1+3	winter	2012	81,5 (90,5)	gap	17,91	0,87	0,60	0,086	10,08	5,74	4,86	3,35	0,48	56,28	32,05
	24.03.12	18.06.12	#4-7	spring		86		13,54	0,51	0,56	0,064	5,93	5,97	3,77	4,17	0,47	43,80	44,09
	18.06.12	12.09.12	#8-11	summer		86		12,90	0,27	0,31	0,046	8,67	3,35	2,09	2,37	0,36	67,21	25,97
	12.09.12	29.12.12	#12-16	fall		107,5		21,10	0,98	0,73	0,097	10,96	7,71	4,62	3,45	0,46	51,94	36,54

906  
907

908

909 Table 3. Correlation coefficients between organic carbon flux and major bulk flux components for the four  
 910 different seasons (lower trap data only). Number of data points (N) and the slopes (s) for the regression lines  
 911 are given as well. Statistically significant values for R<sup>2</sup> at a 99.9% confidence level are indicated in bold.

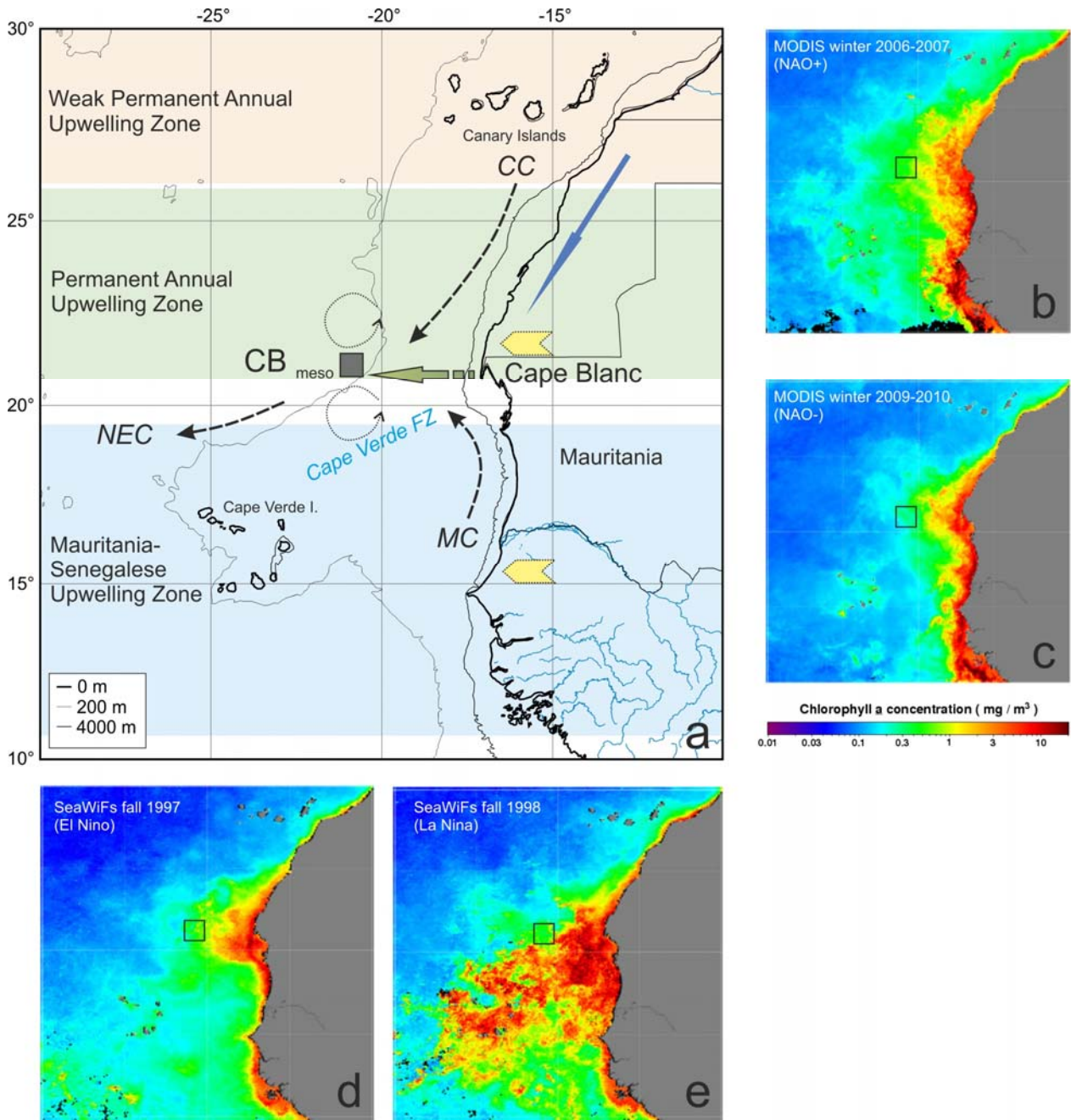
<b>organic carbon</b>	<i>winter</i>	<i>spring</i>	<i>summer</i>	<i>fall</i>
nitrogen	<b>0.96</b> N=16 s=0.13	<b>0.93</b> N=19 s=0.12	<b>0.92</b> N=19 0.12	<b>0.93</b> N=18 0.11
BSi	<b>0.70</b> N=16 s=1.3	<b>0.46</b> N=19 s=1.7	<b>0.63</b> N=19 s=1.4	<b>0.75</b> N=18 s=1.4
carbonate	<b>0.56</b> N=15 s=8.9	<b>0.56</b> N=19 s=10.9	0.16 N=19 s=6.0	<b>0.82</b> N=18 s=13.2
lithogenic (=mineral dust)	<b>0.63</b> N=16 s=6.9	<b>0.53</b> N=19 s=8.5	0.43 N=19 s=5.6	<b>0.67</b> N=18 s=8.6

912

913 Table 4. Summary of important flux changes between 1988 and 2012 which are related to large scale climate  
 914 modes such as NAO and ENSO. The record is divided into six major periods, including the outstanding year  
 915 2005 (see text).

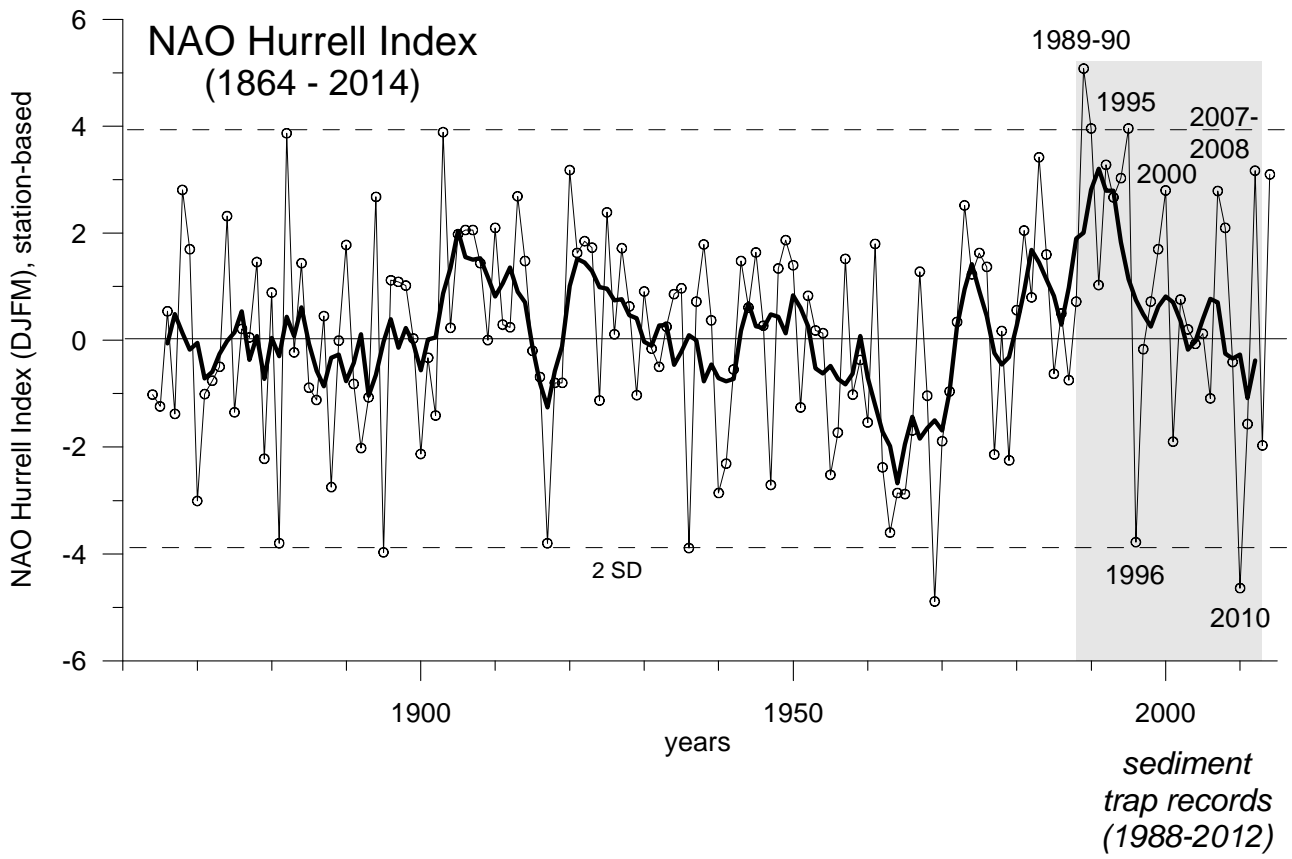
Period/years	1988-1991	1997-1999 El Niño - La Niña	2001-2005/6	2005	2007-2010	2010-2012
<b>FORCING:</b>						
<b>NAO</b>	decreasing	increasing	negative or neutral	neutral	decreasing	increasing
<b>ENSO</b>		strongest ENSO	weak ENSOs	neutral		
<b>FLUX RESPONSE:</b>						
<b>BSi</b>	decreasing	first decreasing, then increasing	episodic peaks	High throughout, except spring	decreasing	increasing
<b>Carbonate</b>	decreasing	generally high, pteropod peaks	major episodic pteropod peaks			
<b>Lithogenic (dust)</b>	decreasing	first decreasing, then increasing		high throughout, except spring	decreasing	increasing

916



917  
918  
919  
920

Fig. 1

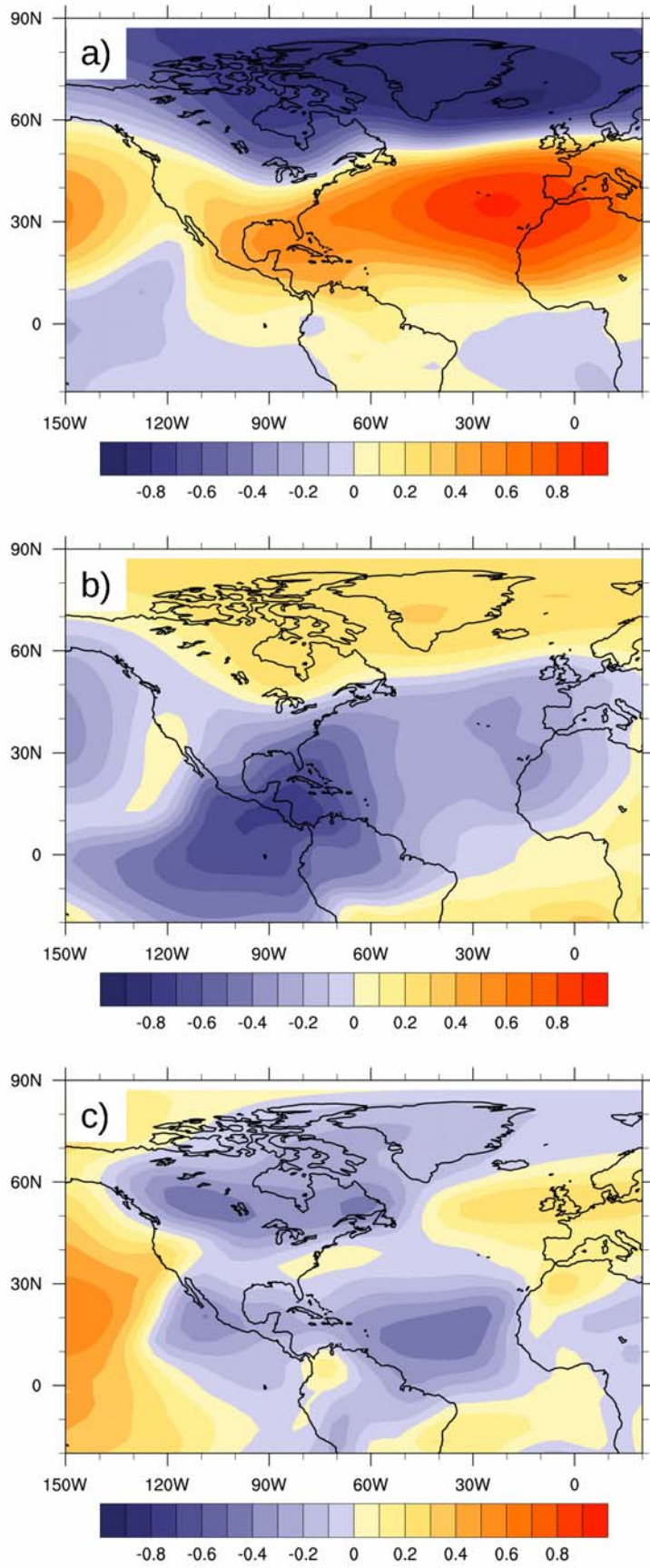


921  
922  
923  
924  
925

Fig. 2.



926

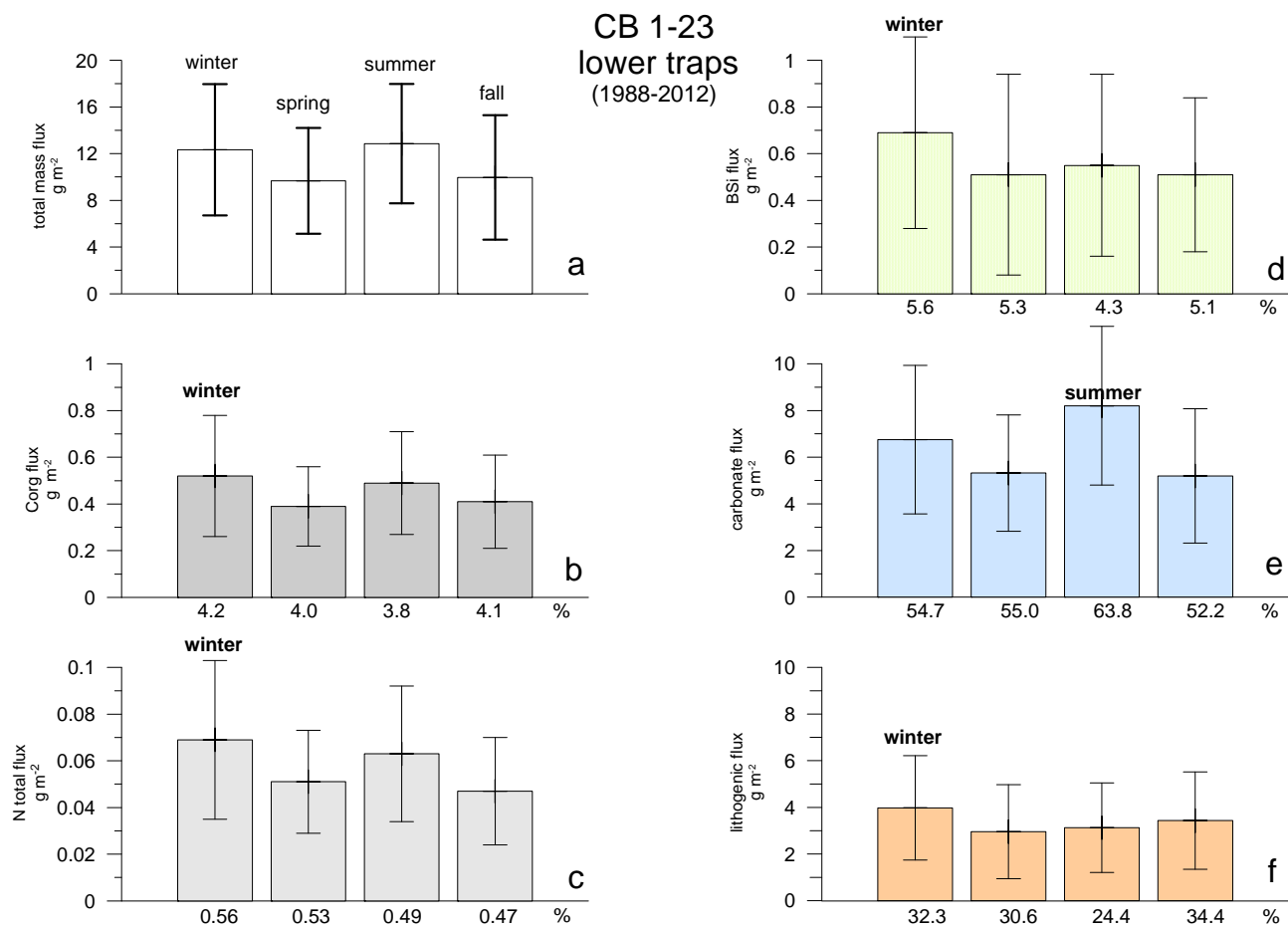


927

928 Fig. 3.

929

930



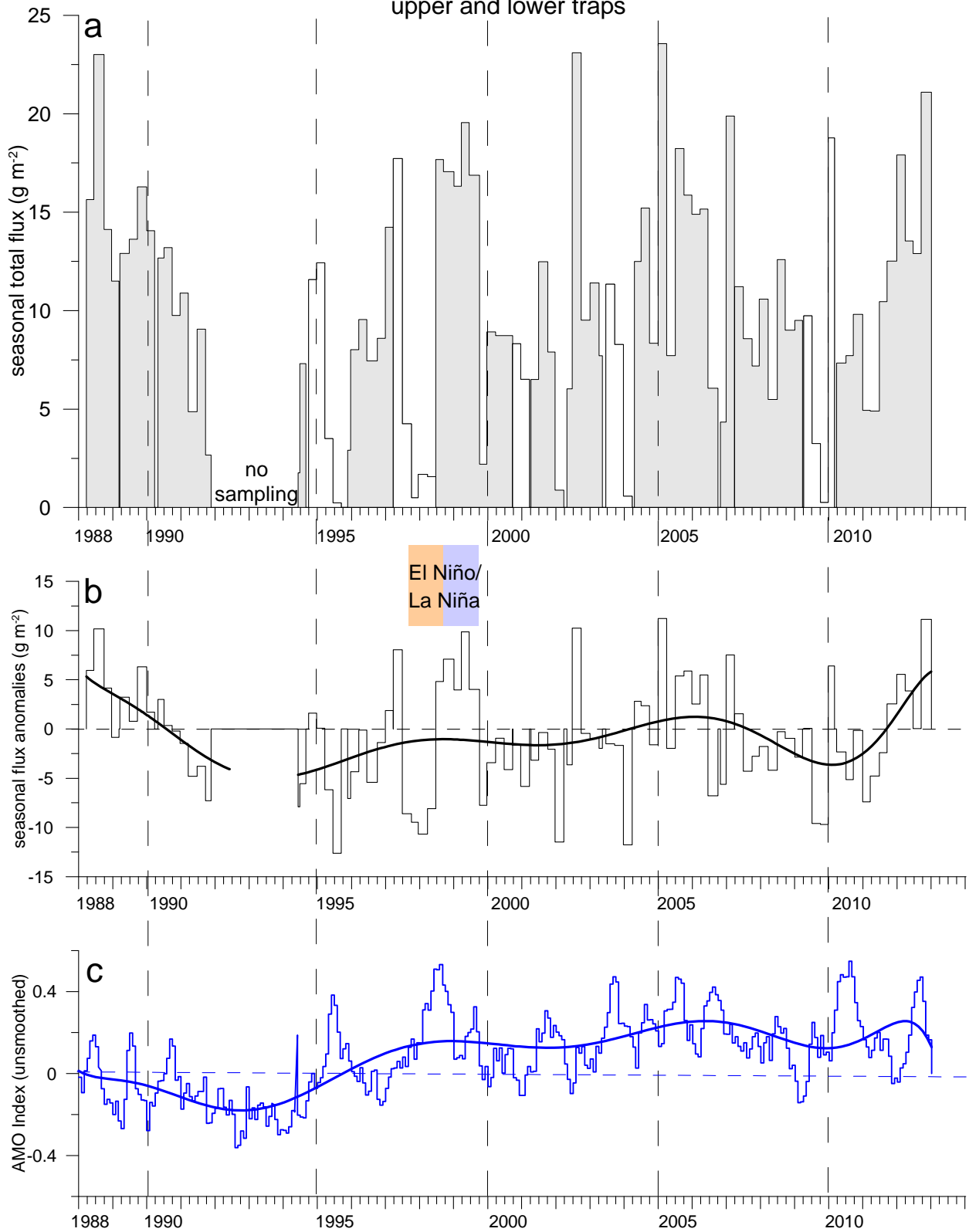
931

932

933 Fig. 4.

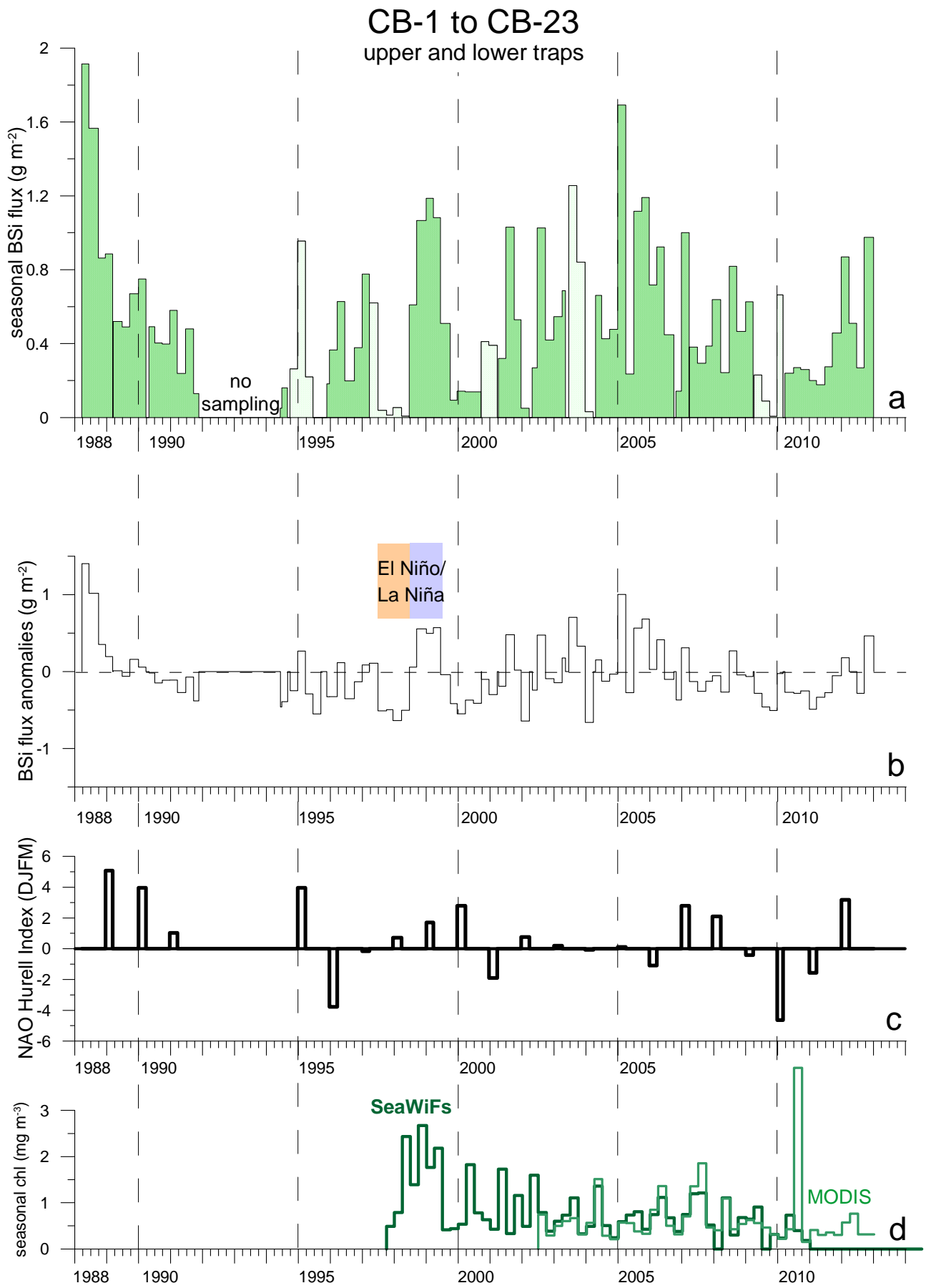
934

# CB-1 to CB-23 upper and lower traps



935

936 Fig. 5.



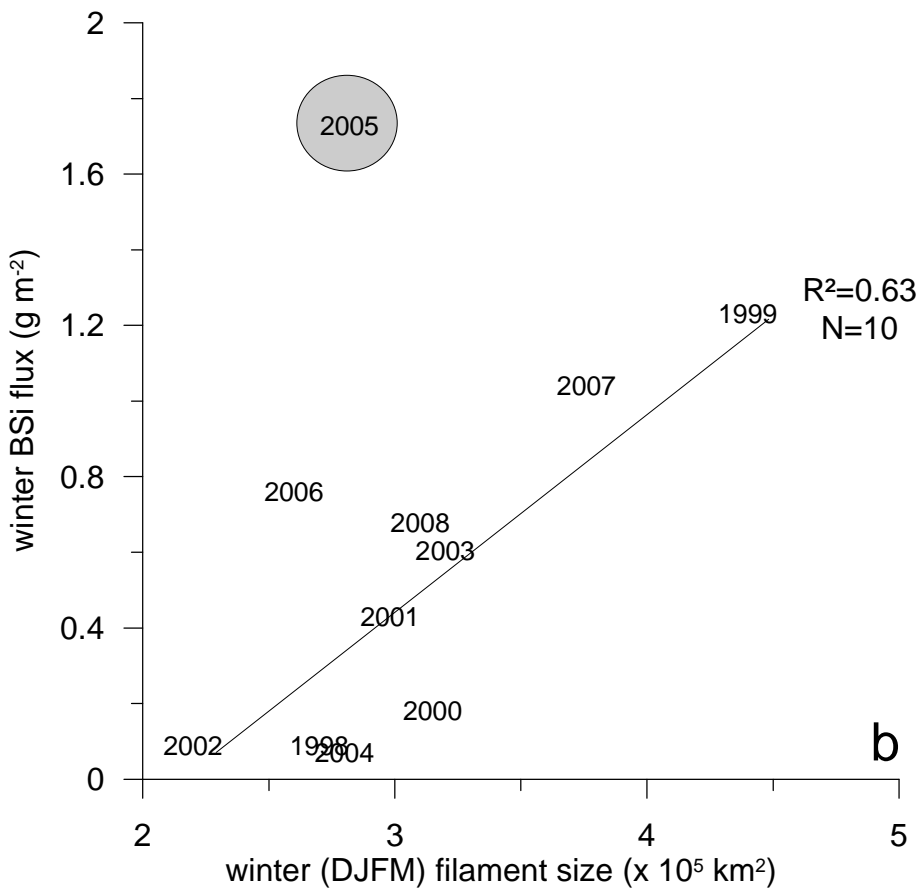
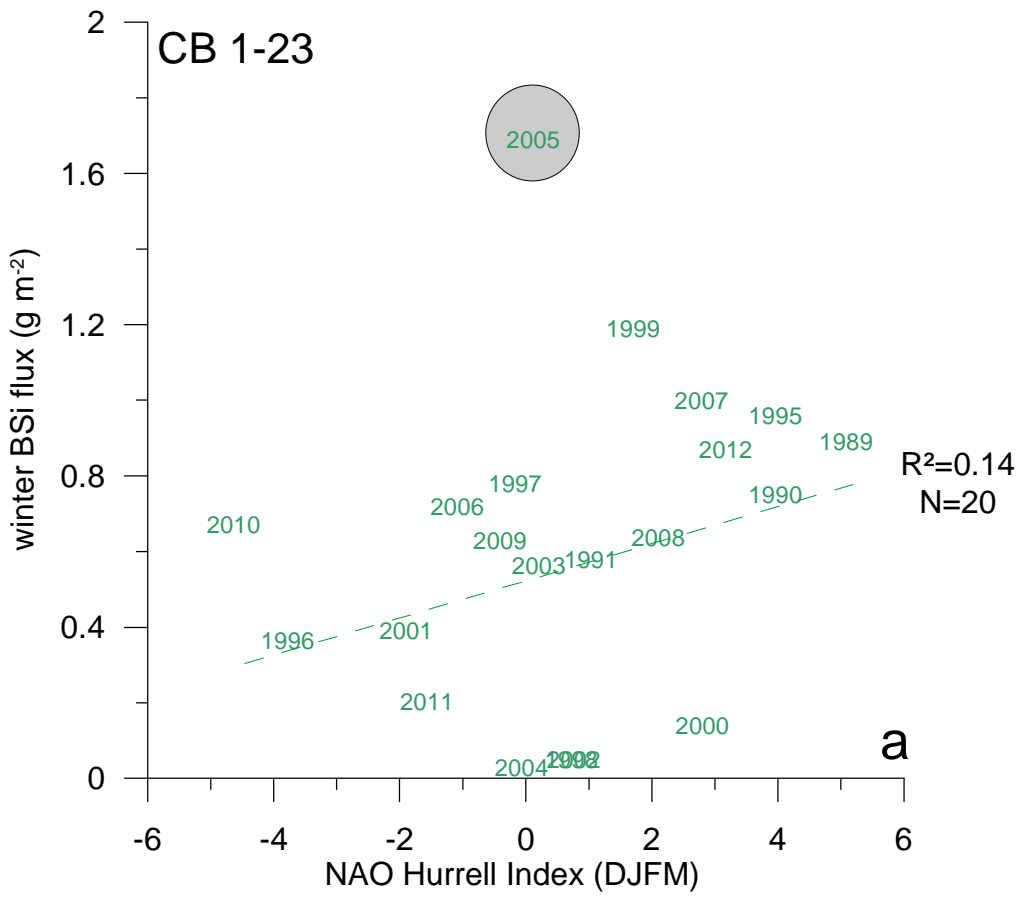
937

938

939

Fig. 6.

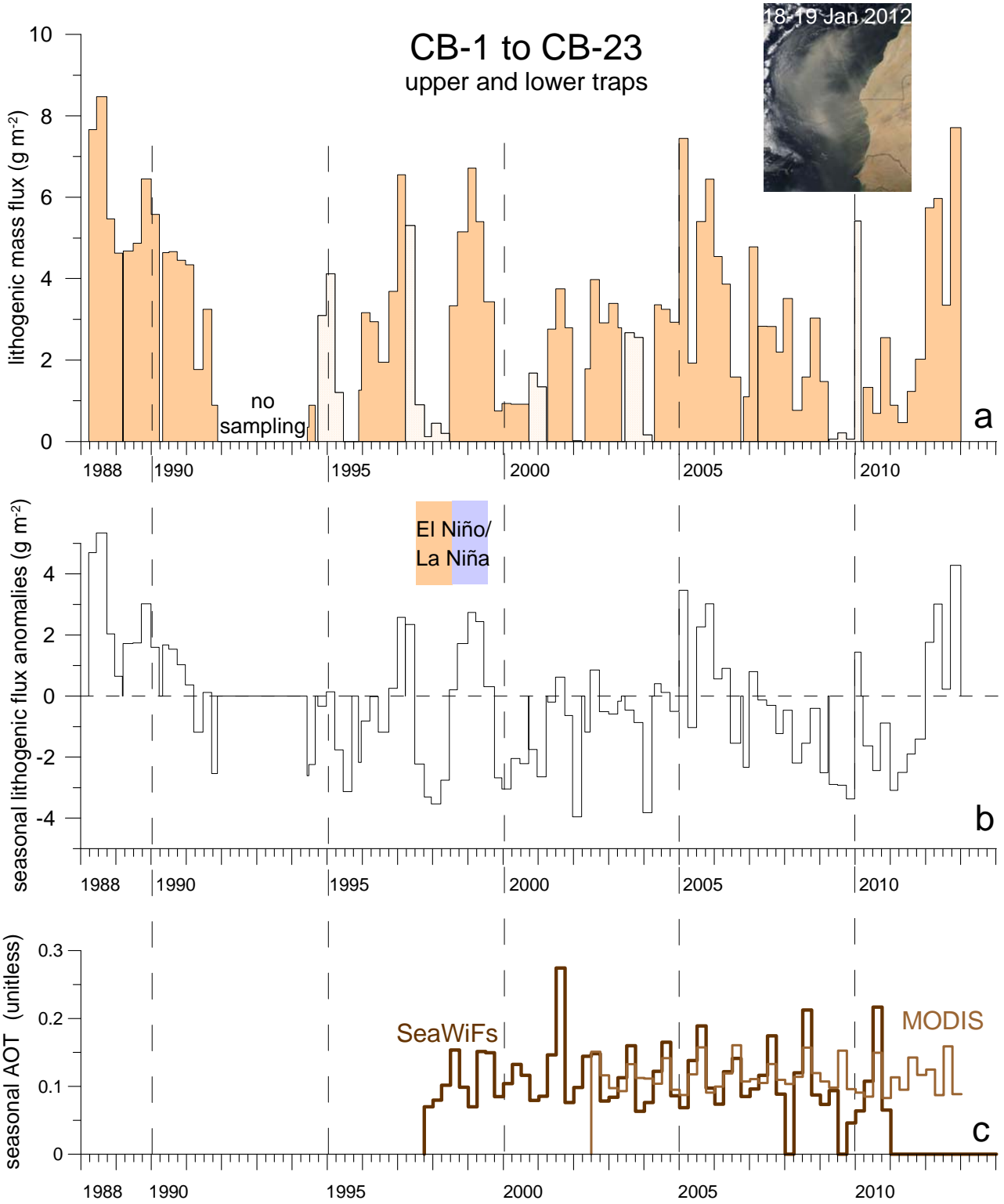
940



941  
942  
943  
944

Fig. 7.

945

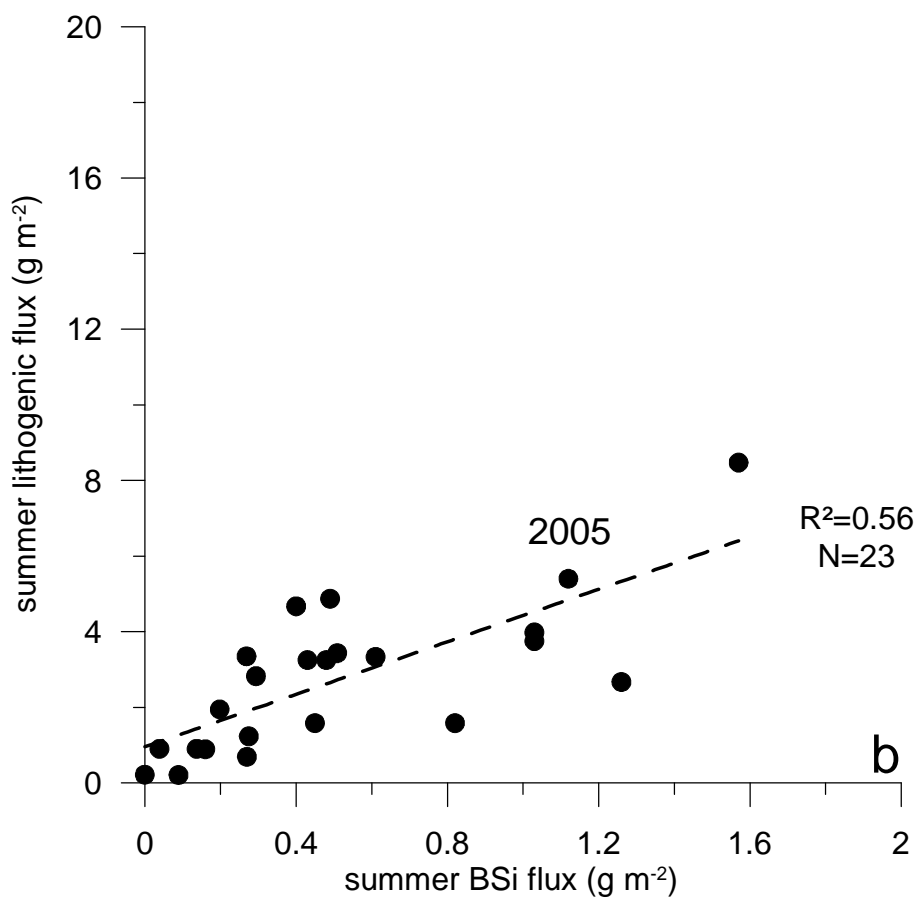
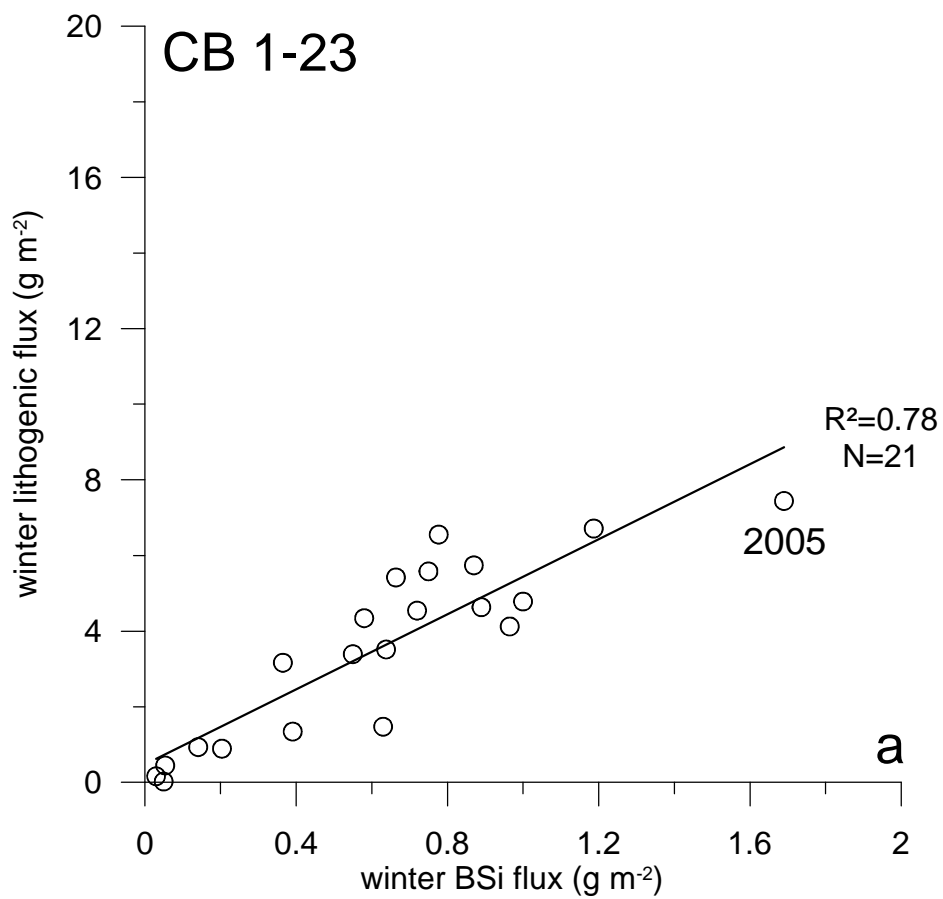


946

947

948 Fig. 8.

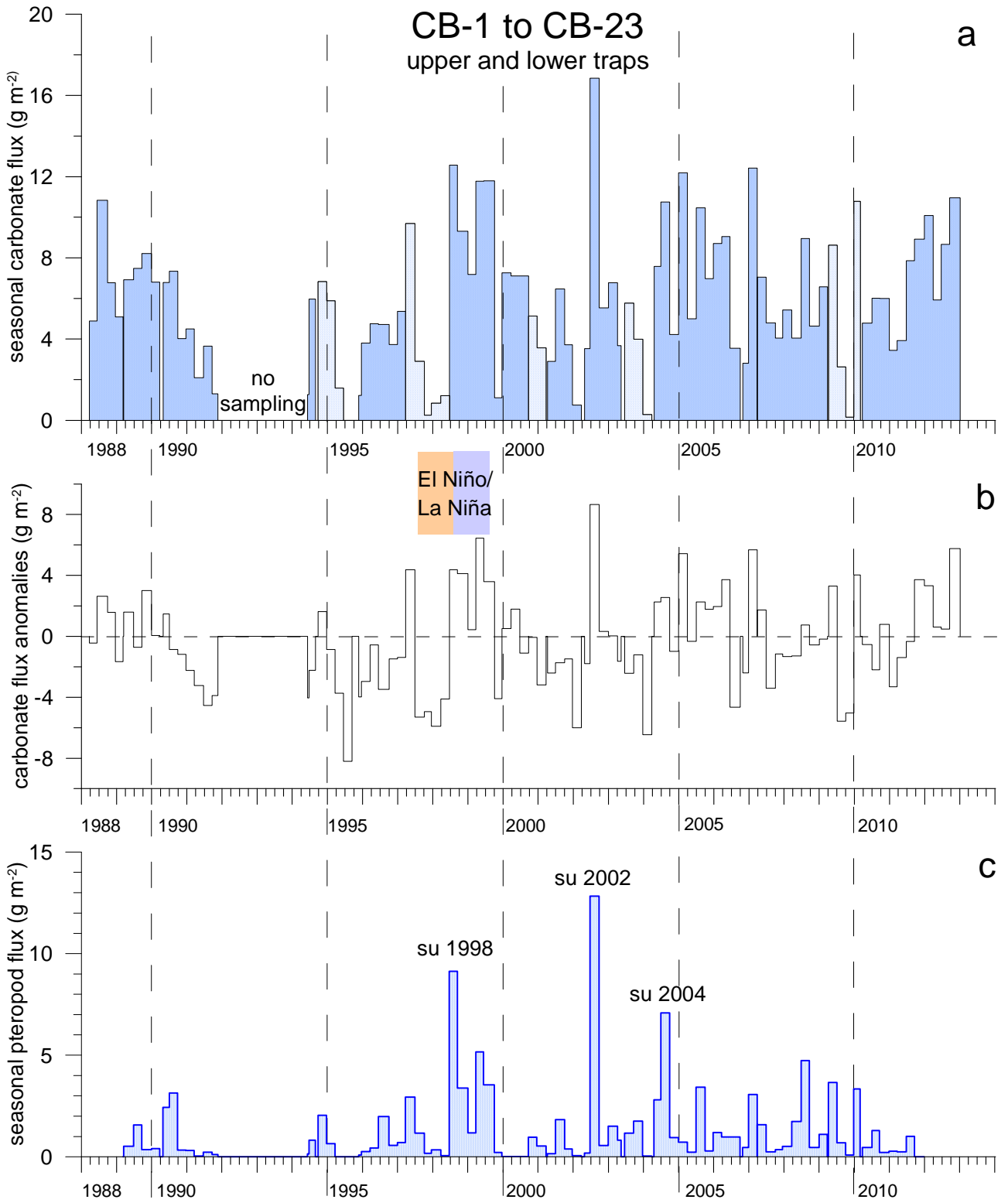
949



950  
951  
952  
953

Fig. 9.

954



955

956

957 Fig. 10.